Physiol Genomics 42: 93–114, 2010.
First published April 6, 2010; doi:10.1152/physiolgenomics.00176.2009.

Compensatory proteome adjustments imply tissue-specific structural and metabolic reorganization following episodic hypoxia or anoxia in the epaulette shark (*Hemiscyllium ocellatum*)

W. Wesley Dowd,[1,2] Gillian M. C. Renshaw,[3] Joseph J. Cech, Jr.,[2] and Dietmar Kültz[1]

Departments of [1]Animal Science and [2]Wildlife, Fish, and Conservation Biology, University of California, Davis, California; and [3]Hypoxia and Ischemia Research Unit, School of Physiotherapy and Exercise Science, Griffith University, Gold Coast Campus, Queensland, Australia

Submitted 19 October 2009; accepted in final form 5 April 2010

Dowd WW, Renshaw GMC, Cech JJ Jr, Kültz D. Compensatory proteome adjustments imply tissue-specific structural and metabolic reorganization following episodic hypoxia or anoxia in the epaulette shark (*Hemiscyllium ocellatum*). *Physiol Genomics* 42: 93–114, 2010. First published April 6, 2010; doi:10.1152/physiolgenomics.00176.2009.— The epaulette shark (*Hemiscyllium ocellatum*) represents an ancestral vertebrate model of episodic hypoxia and anoxia tolerance at tropical temperatures. We used two-dimensional gel electrophoresis and mass spectrometry-based proteomics approaches, combined with a suite of physiological measures, to characterize this species' responses to *1*) one episode of anoxia plus normoxic recovery, *2*) one episode of severe hypoxia plus recovery, or *3*) two episodes of severe hypoxia plus recovery. We examined these responses in the cerebellum and rectal gland, two tissues with high ATP requirements. Sharks maintained plasma ionic homeostasis following all treatments, and activities of Na^+/K^+-ATPase and caspase 3/7 in both tissues were unchanged. Oxygen lack and reoxygenation elicited subtle adjustments in the proteome. Hypoxia led to more extensive proteome responses than anoxia in both tissues. The cerebellum and rectal gland exhibited treatment-specific responses to oxygen limitation consistent with one or more of several strategies: *1*) neurotransmitter and receptor downregulation in cerebellum to prevent excitotoxicity, *2*) cytoskeletal/membrane reorganization, *3*) metabolic reorganization and more efficient intracellular energy shuttling that are more consistent with sustained ATP turnover than with long-term metabolic depression, *4*) detoxification of metabolic byproducts and oxidative stress in light of continued metabolic activity, particularly following hypoxia in rectal gland, and *5*) activation of prosurvival signaling. We hypothesize that neuronal morphological changes facilitate prolonged protection from excitotoxicity via dendritic spine remodeling in cerebellum (i.e., synaptic structural plasticity). These results recapitulate several highly conserved themes in the anoxia and hypoxia tolerance, preconditioning, and oxidative stress literature in a single system. In addition, several of the identified pathways and proteins suggest potentially novel mechanisms for enhancing anoxia or hypoxia tolerance in vertebrates. Overall, our data show that episodic hypoxic or anoxic exposure and recovery in the epaulette shark amplifies a constitutive suite of compensatory mechanisms that further prepares them for subsequent insults.

elasmobranch; proteomics; cerebellum; oxidative stress; preconditioning; cytoskeleton; synaptic plasticity; excitotoxicity

THE EPAULETTE SHARK (*Hemiscyllium ocellatum*) is a rare exception among fully developed vertebrates in its ability to survive severe episodic hypoxia and even several hours of anoxia at tropical temperatures of 25–30°C with no evidence of long-term detriments (67, 71, 84, 85, 113). A few exceptional adult vertebrates such as the crucian carp (*Carassius carassius*) and freshwater turtles (*Trachemys scripta* and *Chrysemys picta*) tolerate much longer anoxic exposures, though these abilities evolved at much colder temperatures (58). Embryos of the annual killifish (*Austrofundulus limnaeus*) survive months of anoxia at 25°C (81), but differences in developmental stage confound comparisons with adult epaulette shark.

The interaction of the lunar and tidal cycles on shallow platforms of the Great Barrier Reef produces an environment in which epaulette sharks are periodically exposed to progressively longer, more severe hypoxia over successive nights. These hypoxic episodes coincide with nocturnal, spring low tides (i.e., new or full moon, Fig. 1) when net ecosystem respiration exceeds oxygen production and the reef crest impedes exchange of seawater with the open ocean. Because anoxic conditions are unlikely to be encountered by this fish in the wild, episodic anoxia tolerance in epaulette sharks possibly represents a byproduct of natural selection for tolerance of severe hypoxia; common mechanisms are often involved in both phenomena.

Many adaptations that confer hypoxia and, especially, anoxia tolerance serve to maintain energetic balance (i.e., ATP levels) in the brain (59). Both ATP-consuming and ATP-producing processes are typically downregulated in response to lack of oxygen in the most tolerant species, a phenomenon known as metabolic depression (31, 98). This process occurs hierarchically within both the entire brain (e.g., downregulation of activity, hearing, and vision centers, the latter in epaulette sharks, 37, 101, 103) and individual neurons [e.g., decreases in energetically expensive processes such as protein synthesis or action potential firing ("spike arrest"), 31, 97]. Selective metabolic depression thus guarantees essential neuronal functions such as ion pumping and membrane polarization (e.g., via activity of Na^+/K^+-ATPase) when ATP production is limited by the lack of oxygen. Similar to other anoxia-tolerant species, epaulette sharks successfully defend brain ATP, ADP, and AMP concentrations following two episodes of anoxia spaced 24 h apart (85). Adenosine levels are significantly elevated in the brains of these fish after the second 50 min episode of anoxia. Notably, the brain energy charge decreases when sharks are treated with the adenosine receptor antagonist aminophylline (85), suggesting that adenosine contributes to epaulette shark metabolic depression during anoxic episodes, as it does in other anoxia-tolerant species (59). Although tissues other than brain must also regulate their

Address for reprint requests and other correspondence: W. W. Dowd, Hopkins Marine Station of Stanford Univ., 120 Oceanview Blvd., Pacific Grove, CA 93950 (e-mail: wwdowd@stanford.edu).

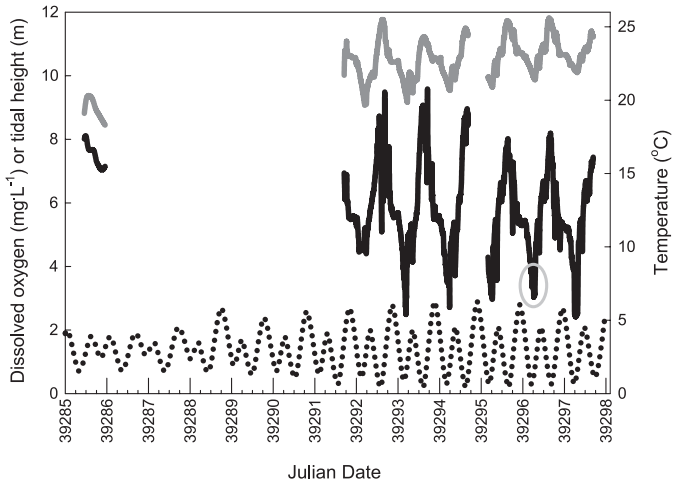

Fig. 1. Profiles of dissolved oxygen (black line) and water temperature (dark gray line) in relation to tidal height (dotted line) on the Heron Island reef platform for both neap tides (from flood tide through nocturnal low tide on July 22, 2007; *left*) and spring tides (7 day plot from July 28 to August 3, 2007; *right*). Severe reductions in dissolved oxygen coincide with nocturnal, spring low tides. Large *x*-axis ticks indicate midnight; smaller ticks represent 6 h intervals. Light gray circle denotes the time at which the field blood samples were collected. Note that these measurements were taken in Austral winter; oxygen limitation is likely to be even more severe at higher summer temperatures.

metabolic processes during and after oxygen limitation, the compensatory strategies of other tissues in this and other hypoxia- and anoxia-tolerant species have received far less attention.

Just as critical as the need to survive periods of oxygen limitation is the ability to cope with subsequent rapid reoxygenation. The return to normoxic conditions in mammalian systems coincides with bursts in the generation of reactive oxygen species (ROS) or reactive nitrogen species (RNS) (i.e., oxidative stress). The associated macromolecular damage and cell death (necrosis and/or apoptosis) is commonly referred to as reoxygenation/reperfusion injury (reviewed in Ref. 54). Recent work has demonstrated that elevated ROS formation may occur during hypoxia as well (54, 56, 57). Thus, the epaulette shark's survival of episodic hypoxia on the reef platform (and episodic anoxia in the laboratory) may in some ways be more relevant than long-term anoxia tolerance to biomedical interest in ischemia/reperfusion, due to this species' apparent ability to repeatedly suppress or minimize reoxygenation injury.

Due to the repeated, episodic nature of hypoxia in the epaulette shark's habitat, the reef platform has been referred to as a natural "hypoxic preconditioning environment" (71). By the term preconditioning (or conditioning hormesis, 9) we refer to the common phenomenon in which exposure to an initial stress elicits physiological and biochemical responses (the preconditioned phenotype) that offer protection against a subsequent, more severe stress (the preconditioning outcome). This preconditioning outcome typically manifests in the form of reduced tissue or molecular damage and/or increased survivorship. Although definitive evidence for a preconditioning outcome as defined above is lacking in the epaulette shark, this may be moot given that this species likely represents a "constitutively preconditioned" (sensu 66) model of hypoxia and anoxia tolerance. Accordingly, epaulette sharks raised in captivity and thus naïve to oxygen limitation are also tolerant of episodic anoxia (13).

Clearly some of the pathways that prevent neuronal and organismal death after several hours of severe hypoxia or anoxia at tropical temperatures, as well as those conferring the ability to suppress reoxygenation injury, must be constitutively expressed in this species. However, novel or enhanced protective mechanisms that confer increased damage resistance may also be induced by preexposure to oxygen limitation. The relative costs and benefits of these two strategies should depend on the degree, frequency, and predictability of low oxygen conditions experienced in the wild relative to the costs of synthesizing, stabilizing, and degrading the necessary proteins and repairing damage. Several lines of evidence suggest that a preconditioned phenotype is activated by hypoxic preexposure in the epaulette shark. Laboratory exposure to multiple hypoxic episodes reduces the organismal aerobic metabolic rate and reduces the critical oxygen tension for maintenance of aerobic metabolism (71, 89). Within the epaulette shark brain, the same repeated hypoxia protocol promotes neuronal aerobic hypometabolism via a decrease in abundance of the tricarboxylic acid cycle enzyme citrate synthase (68) and results in increased localized concentrations of the inhibitory neurotransmitter GABA, particularly in nuclei of the brainstem and cerebellum (67). These adjustments may reduce both ATP turnover and excitatory stimulation and thus provide neuroprotection. Yet, we possess a minimal understanding of the molecular mechanisms underlying these and other responses to oxygen limitation in the epaulette shark brain and other tissues.

Given the previous evidence for prolonged preconditioning in field-acclimatized epaulette sharks (and in mammalian models, 4, 99), the periodic and incremental nature of hypoxia on reef platforms due to its dependence on the lunar cycle, and the likely involvement of protein synthesis in late ischemic preconditioning (87), we anticipated that at least some of the epaulette shark's compensatory response mechanisms are inducible and would be detectable after reoxygenation (e.g., 117). Therefore, in this study we exposed epaulette sharks to controlled anoxic, hypoxic, and repeated hypoxic treatments plus 2 or 24 h of normoxic recovery to assess their responses to no vs. low oxygen and to determine whether these responses vary between one and more than one hypoxic episodes. Because proteins perform the majority of cell functions, we used two-dimensional gel electrophoresis and mass spectrometry-based proteomics approaches to quantify molecular responses to oxygen limitation. Measures at the proteome level integrate changes in transcription, mRNA stability, and protein turnover in response to stressors (5, 19, 46). We focused on the 24 h recovery time point for our proteomics analyses for three reasons: *1*) reoxygenation induces as or more severe damage as the period of oxygen limitation (5, 56); *2*) compensatory stress response mechanisms may be more potent during the recovery period than during the actual stress period (5, 49); and *3*) hypoxic episodes are naturally spaced 24 h apart on the reef platform. Thus, our proteomic data represent the phenotype at the time when the next stressful episode would likely be encountered. This 24 h lag also coincides with the onset of the delayed phase of ischemic preconditioning in mammalian models (e.g., 4).

We first examined responses to oxygen limitation in the cerebellum, which controls critical organismal functions (including reflex coordination) and is highly vulnerable to oxygen limitation in most species. Cerebellar activity appears to be downregulated during anoxia in the epaulette shark, as evidenced by the reversible loss of a righting reflex (85). We anticipated that adaptive molecular responses to oxygen limitation might occur in pathways related to energy metabolism, redox balance and ROS neutralization, protein stabilization and repair, and apoptosis/cell cycle. Thus, our expectation was that patterns of protein abundance in these pathways would vary depending on the hypoxic or anoxic exposure regime. We then asked whether oxygen limitation elicits similar or divergent responses in another tissue that performs a vital organismal function. The elasmobranch rectal gland uses significant amounts of aerobically derived ATP to fuel the high Na^+/K^+ ATPase activity that drives excretion of NaCl for ionoregulation (22), but it may also have substantial anaerobic capacity (110).

In concert with the proteomics data from both cerebellum and rectal gland, we assessed a number of indicators of metabolic and physiological status in the same individuals and tissues. At the organismal level this included measures of ventilation rate during episodes of oxygen limitation, circulating plasma glucose (a favored metabolic fuel of elasmobranch brain and rectal gland), and plasma lactate (the primary end product of anaerobic glycolysis). We anticipated that there might be some breakdown or selective downregulation of the rectal gland's salt and extracellular volume homeostatic functions (assessed here via measurements of plasma ion concentrations) with oxygen limitation. At the biochemical level, we measured the activity of Na^+/K^+-ATPase, a major ATP sink in both tissues (albeit in support of different functions), to determine whether oxygen limitation and recovery elicits a decrease in ion pumping capacity. The combined activities of the apoptotic effector enzymes caspases 3 and 7 were used as an indicator of apoptosis, the programmed cell death that may result from exposure to excessive stress (46). Finally, we measured levels of glutathione to determine whether epaulette sharks have high constitutive expression of this ROS scavenger or whether the total glutathione pool could be regulated as part of the response to oxygen limitation. Based on these integrative data, we outline some of the common, treatment-specific, and tissue-specific mechanisms involved in the epaulette shark's response to episodic anoxia and hypoxia plus reoxygenation.

MATERIALS AND METHODS

Animal Capture and Maintenance

Epaulette sharks ($n = 42$, mean 356 ± 21 g, range 69–646 g) were collected by hand at low tide on the reef platform surrounding Heron Island Research Station (23.4500°S, 151.9167°E) on the Great Barrier Reef. Sharks were transported in mesh bags to an outdoor 5,000-liter holding tank, where they were maintained at natural winter photoperiod, temperature (range 16.5–20°C), and salinity (35.5–37 ppt), for 37 to 158 h (mean 84 ± 7) prior to experimentation. Dissolved oxygen in the aerated holding tank averaged 6.9 ± 0.1 mg O_2/l (parts per million) (>90% air saturation). The sharks were not fed in captivity. Each day 1,000 liters (~20% of the tank volume) of seawater were exchanged in the holding tank with fresh seawater. There were no differences in body mass (356 ± 21 g, $P = 0.23$) or total length (52.9 ± 1.2 cm, $P = 0.10$) among the treatments. The animals in the three hypoxic treatments were held in captivity for a shorter period before the experiments (37 ± 2 h) than those in the anoxic treatments (88 ± 9 h). This research was carried out under the auspices of the Great Barrier Reef Marine Parks Authority permits G07/24973.1 and G07/23338.1.

Anoxic and Hypoxic Exposures

Anoxic and hypoxic exposures were conducted in 65-liter glass aquaria with one animal per aquarium. Aquaria were fitted with clear plastic covers to minimize gas diffusion while allowing ambient light to enter, and the sides were wrapped in black plastic to prevent visual disturbance of the sharks. The sharks and treatments were randomly assigned to each of 10 aquaria each day to prevent systematic errors in the experimental design due to tank effects. Experiments were conducted at ambient temperature (16–21°C. mean 18.9°C), which approximated the temperatures observed on the reef platform during the study. Compressed nitrogen gas was bubbled into the chambers via two diffuser stones to create anoxic conditions (<0.1% air saturation, operationally defined as <0.03 mg O_2/l) or hypoxic conditions (~5% air saturation, operationally defined as 0.39 ± 0.03 mg O_2/l). Control normoxic tanks (operationally defined as 6.53 ± 0.10 mg O_2/l) were aerated using a single diffuser stone and air pump. A small aquarium pump was used to ensure a homogeneous environment within each aquarium. Oxygen concentrations were determined with a TPS WP-82Y dissolved oxygen meter fitted with a YSI 5739 probe, which was calibrated daily in air and zero-oxygen solution (saturated Na_2SO_3 solution).

The sharks were subjected to one of eight treatments (Fig. 2), in which A1 represents exposure to anoxia until time of loss of the righting reflex (T_{LRR}) (85), A2 represents a second 50 min episode of anoxia after A1 and following 24 h of recovery, H1 and H2 similarly represent one or two 2 h episodes of hypoxia separated by 24 h normoxic recovery, C1 represents 2 h of normoxia (control), and the subsequent times indicate the recovery period in the holding tank before sampling: A1 + 2 h ($n = 5$), C1 + 2 h ($n = 4$), A1 + 24 h ($n = 5$), C1 + 24 h ($n = 5$), A1 + A2 ($n = 5$), H1 + 24 h ($n = 6$), H1 + H2 + 2 h ($n = 6$), H1 + H2 + 24 h ($n = 6$). The repeated low oxygen exposures (i.e., A1 and A2, H1 and H2) were spaced 24 h apart to mimic the periodicity of dissolved oxygen fluctuations on the reef platform (Fig. 1). The T_{LRR} was chosen as the endpoint for the A1 anoxia experiments because it may indicate the onset of a deeper phase of metabolic depression (85).

Animals were identified from photographs of the unique spot patterns on the dorsal region. At the beginning of an experiment, the sharks were removed from the holding tank and placed into the

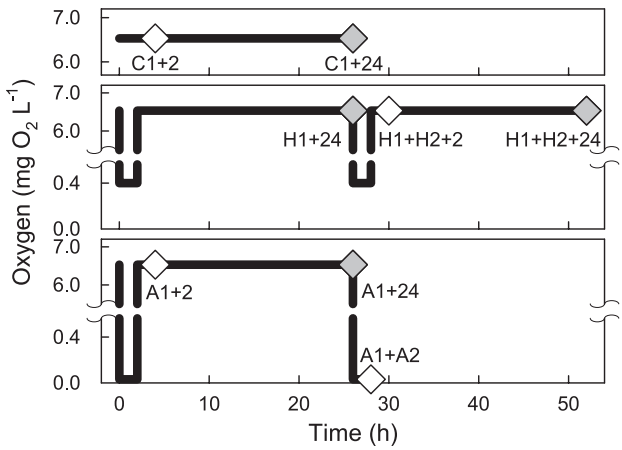

Fig. 2. Schematic of the experimental design showing oxygen concentrations over time. *Top*, controls; *middle*, hypoxia; *bottom*, anoxia. Diamonds indicate the sampling time points. Gray diamonds represent the 4 time points included in the proteomics analysis.

appropriate anoxic or hypoxic aquarium (i.e., they were subjected to acute low oxygen conditions as in previous studies) (13, 68, 85). Gill ventilation rates (rhythmic gill slit openings in beats per min) were determined every 15 min. In the anoxia treatments, once the ventilation rate had stabilized at a low level (typically 3–10 beats per min after ~100 min), each animal was subsequently tested for reflex responses every 15 min until the T_{LRR} as in Renshaw et al. (85). The animal was then returned to the holding tank for the +2 h or +24 h recovery period. Most sharks recovered swimming ability within 3–5 min of removal from anoxia, many within seconds. Control and hypoxia treatment animals were handled in a similar fashion.

At the appropriate sampling time, two 0.9-ml blood samples were drawn from each animal via the caudal vein into a heparinized syringe. Animals were then euthanized with an overdose of benzocaine (~80–100 mg/l), and sex, weight, and length were determined. The blood was centrifuged at 3,800 rpm for 5 min at 4°C, after which the plasma and red blood cell pellet were separated and frozen in duplicate in liquid nitrogen. The entire rectal gland and one half of the cerebellum were quickly dissected out and snap-frozen in liquid nitrogen; the brain samples were frozen within 4 min. All plasma and tissue samples were shipped on dry ice to the University of California, Davis and then stored at −80°C until analysis.

For comparison with the experimental animals, we also collected field blood samples from epaulette sharks ($n = 6$; 4 females, 2 males) on the Heron Island reef platform during a hypoxic nocturnal, spring low tide (2–4 AM, Fig. 1).

Plasma Lactate, Glucose, and Electrolytes

The concentrations of L-lactate and D-glucose (mmol/l) were determined in triplicate on a YSI 2700 Biochemistry Analyzer. Plasma samples were also analyzed in triplicate for Na^+ and K^+ concentrations (mmol/l) by flame photometry (Instrumentation Laboratory 343), Cl^- concentration (mmol/l) using a chloride titrator (Labconco Digital Chloridometer), and osmolality (mOsmol/kg) using a vapor pressure osmometer (Wescor Vapro 5520).

Enzyme Activity and Glutathione Assays

Na^+/K^+ ATPase activity. The activity of Na^+/K^+ ATPase per mg of total protein was determined in triplicate in rectal gland and brain (cerebellum) homogenates following the methods of McCormick (64), as applied to elasmobranchs by Piermarini and Evans (79a).

Caspase 3/7 activity. We determined the combined activity of caspases 3 and 7, two proteases that are early effectors of apoptosis, in duplicate using a microplate-based luminescent assay (Caspase Glo 3/7 assay kit, Promega) modified for tissue homogenates (18, 41). Brain and rectal gland tissues were homogenized in nondenaturing lysis buffer (10 mM Tris·HCl pH 7.5, 100 mM NaCl, 0.1 mM EDTA, 0.2% Triton-X 100). Caspase 3/7 activity was normalized to total protein, as determined by a bicinchoninic acid (BCA) assay (Pierce). Due to limited tissue mass, we had insufficient sample sizes to carry out statistical analyses on the rectal gland caspase data.

Glutathione. The level of reduced glutathione (GSH) may decrease during oxidative stress (e.g., during ROS formation following reoxygenation) as GSH donates a reducing equivalent to reactive oxygen species or oxidized proteins and itself is oxidized to GSSG. We measured the level of GSH in brain homogenates (in the same buffer as used for caspase 3/7 activity) in duplicate using a microplate-based luminescent assay (GSH-Glo assay, Promega). We treated two additional wells of each homogenate with 1 μl of the reducing agent Tris(2-carboxyethyl)phosphine (TCEP; 900 μM) to convert all GSSG back to GSH, allowing us to determine the size of the total glutathione pool (GSH + GSSG) as well as the fraction of the glutathione pool in the oxidized and reduced states after each treatment. Luminescence was converted to GSH concentration based on a standard curve created by serial dilution of a 5 mM GSH standard in the homogenization buffer per the manufacturer's instructions. GSH was normalized to total protein, as determined by a BCA assay (Pierce).

Statistical Analyses of Physiological and Biochemical Data

In most cases treatment group means were compared using one-way ANOVA followed by Tukey's honestly significant difference post hoc test. Lactate and glucose data were first power transformed to satisfy the homogeneity of variances and normality assumptions. Data that could not be transformed to meet the ANOVA assumptions were analyzed with a Kruskal-Wallis (K-W) nonparametric test. Data for percentage reduced GSH were arcsine-square-root transformed for proportions. Significance level in all cases was set at $\alpha = 0.05$. The ventilation rate data were compared among treatments by fitting the data to separate log-linear regression curves for each treatment using Gauss-Newton iteration. Analyses were performed in Statistica 6.1 (StatSoft).

Proteomics

Two-dimensional gel electrophoresis and image analysis. Proteins regulated by exposure to anoxia or hypoxia in the epaulette shark cerebellum and rectal gland were identified using two-dimensional gel electrophoresis and tandem mass spectrometry following previously established methods (18, 19, 51). We selected the four 24-h recovery time points (Fig. 2) for proteomics analysis. Briefly, proteins were extracted from tissue homogenates in ice-cold RIPA buffer, precipitated in acetone with 10% trichloroacetic acid, loaded (1 mg per sample for cerebellum; 0.75 mg for rectal gland) onto 18-cm immobilized pH 3–10 nonlinear gradient strips (Bio-Rad) by passive overnight rehydration at 4°C, separated in the first dimension by isoelectric focusing, reduced with dithiothreitol and iodoacetamide, and then run on 16-cm second dimension SDS-PAGE gels, all as previously described (18, 19, 107). Two-dimensional gels were stained with Coomassie brilliant blue G250, destained in purified water, and then scanned for densitometry (5, 18, 19, 107). The individual gel images (one gel per individual for both cerebellum and rectal gland) were manually aligned, fused into a master gel image for each tissue, and quantified using Delta 2D software (v3.6, Decodon, Greifswald, Germany) as in Ref. 19. Because no samples were pooled, our data approximate the true biological variability.

Proteomics data analysis. Protein expression levels on individual two-dimensional gels from control, anoxia, and hypoxia treatments were normalized by dividing each spot's intensity on a given gel by the total intensity of all outlined spots on that gel. Treatment spot intensities were then compared with control values using a *t*-test in Delta 2D software (18, 19). Protein spots whose abundance changed significantly ($P < 0.05$) and with an expression ratio >2 (increased by >100%) or <0.5 (decreased by >50%) were processed for mass spectrometry identification, where the expression ratio equals the mean spot volume in a given treatment's gels divided by the mean spot volume in the control gels. These ratios equate to a $\log_{10}$-ratio change of ± 0.30. Because very few spots met these strict criteria, we expanded the analysis to include spots with $P < 0.05$ and an expression ratio <0.67 or >1.5 (i.e., $\log_{10}$-ratio of ± 0.18).

In addition, we performed a partial least squares discriminant analysis (PLS-DA) using SIMCA-P+ software (Umetrix, Umeå, Sweden). This multivariate statistical technique is a regression extension of principal components analysis (PCA) that maximizes the amount of among-groups variation explained by the first components. This technique outperforms PCA, which maximizes the total amount of variation in the dataset explained by the first components regardless of treatment group membership (42, 114). The PLS-DA modeling approach reveals important expression changes in noisy, highly collinear datasets that may be missed by univariate tests such as a *t*-test (42, 78). Based on the full PLS-DA model with all protein spots included, we performed a variable importance in the projection (VIP) analysis. The VIP is a relative measure of the global importance of a

particular feature (i.e., protein spot); spots with high VIP scores are most relevant to distinguishing among the treatment groups. The top 5% of VIP scores (49 spots for brain; 38 spots for rectal gland) were used to fit reduced PLS-DA models for each tissue, following a feature-selection approach applied to microarray data (78) and recently supported by simulation studies (75). These spots in the top 5% of VIP scores were also picked for mass spectrometry analysis.

Mass spectrometry and bioinformatics database searches. Protein spots of interest were excised in duplicate using a 0.5 mm spot puncher and digested overnight at 37°C with mass spectrometry-grade trypsin (Promega). The resulting peptide fragments were eluted from gel pieces by washing twice in 60% acetonitrile:1% trifluoroacetic acid (TFA). The peptide solution was then dried in a SpeedVac and resuspended in 1% TFA. The peptides were desalted and concentrated using μC18 ZipTips (Millipore). The final eluted peptides were spotted in 0.5 μl increments on a stainless steel MALDI target, and overlaid with α-cyano-4-hydroxycinnamic acid matrix (18, 19). Peptides were analyzed on an Applied Biosystems 4700 Proteomics Analyzer MALDI-TOF-TOF tandem mass spectrometer (Foster City, CA) as previously described (18, 19, 51). Peak lists from the resulting MS and MS/MS spectra were searched jointly against the NCBI non-redundant database using the Mascot search algorithm (http://www.matrixscience.com, 79) with mass error tolerances of 50 and 100 ppm for MS, 0.3 and 0.5 Da for MS/MS, and fixed modifications of cysteine residues (carbamidomethylation) and variable oxidation of methionine residues. The MS/MS spectra were also submitted for automated de novo peptide sequencing analysis to PEAKS Studio v4.5 software (Bioinformatics Solutions, Toronto, Canada) (60), with the same criteria as for Mascot. The resulting de novo amino acid sequences for the tryptic peptides were then searched against the NCBI nonredundant database using the PEAKS proprietary search engine. Consensus protein identifications were determined (in duplicate) based on both Mascot and PEAKS scores and from both postsource decay (PSD) and collision-induced dissociation (CID) MS/MS spectra. Matches solely from de novo sequencing scores were only accepted when >1 peptide matched to the protein. When possible, matches were confirmed by general agreement of molecular mass (M_r) and isoelectric point (p*I*) between the database match and the protein spot of interest on 2D gels. However, because many proteins have not been sequenced in elasmobranchs, this is not always possible.

Pathway and molecular network analyses. To aid in the development of functional hypotheses consistent with the proteomics data, the lists of epaulette shark proteins were analyzed separately for cerebellum and rectal gland using Ingenuity Pathways Analysis (IPA) software (Ingenuity Systems, http://www.ingenuity.com). Identifiers for the mouse or human homologs of the identified epaulette shark proteins (from both the *t*-test and VIP analyses) and the corresponding expression ratios and *P* values for each treatment were uploaded into IPA. Lists of significantly represented (based on right-tailed Fisher's exact test) molecular functions [Gene Ontology (GO; http://www.geneontology.org) biological process annotations plus manually added annotations] and canonical cellular pathways were generated for each treatment. The lists of protein identifiers were then overlaid onto the IPA knowledge base global molecular network. Molecular interaction networks containing the anoxia or hypoxia-regulated proteins were algorithmically generated based on their specific connectivity, with each network assigned a statistical likelihood score (10). We first created a master network for each tissue containing all of the proteins of interest (i.e., those that met the *t*-test or PLS-DA VIP criteria in any treatment). The expression ratios for each treatment were overlaid onto this master network to enable direct, visual comparison of the expression changes across treatments.

RESULTS

Time to Loss of Righting Reflex

The time to loss of righting reflex varied considerably (69–258 min) among the experimental animals in anoxia, but there were no systematic differences among the three A1 treatments (A1+2 h, A1+24 h, A1+A2) in T_{LRR} ($P = 0.27$, grand mean 142 ± 16 min). The variation in T_{LRR} was not correlated with body mass ($P = 0.80$), time in captivity (i.e., by potential loss of energy stores) ($P = 0.25$), or the time of day that the experiment started ($P = 0.51$); there was also no difference between the sexes ($P = 0.39$). Thus, these data can best be explained as individual differences. Compared with an earlier study (85), the T_{LRR} in anoxia was significantly longer in our A1 treatments (142 min at 18.9°C vs. 46 min at 28°C).

Ventilation Rate Decreases Rapidly in Anoxia but not Hypoxia

Ventilation rate was elevated in all treatments initially, most likely reflecting handling stress incurred while placing the animals in the chambers. Ventilation frequency in the control animals after ~60 min was similar to that observed in the holding tank and in the wild (~16–19 beats/min). Ventilation rate decreased faster and to lower levels in the three A1 anoxia treatments than in the controls (Fig. 3). The 95% confidence intervals for the slope of the log-linear Gauss-Newton fit overlapped among the three A1 treatments (A1+2: −22.2 to

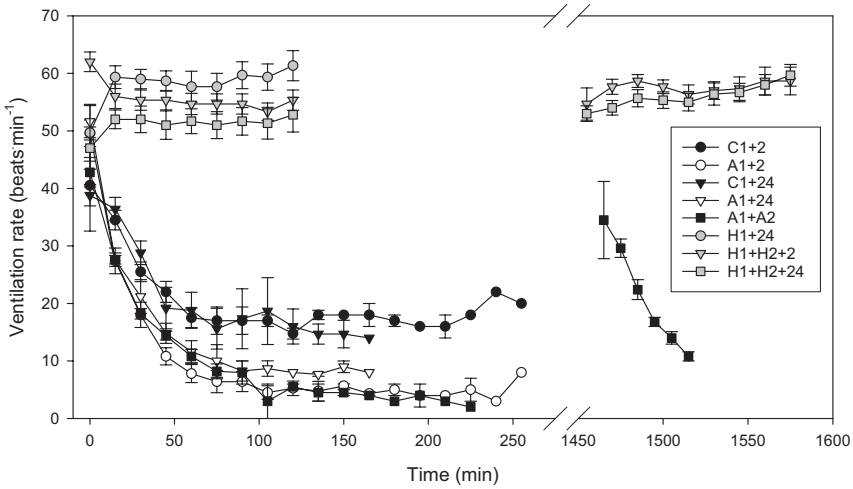

Fig. 3. Ventilation frequency (beats/min) of epaulette sharks following transfer to anoxic (A1 or A2), hypoxic (H1 or H2), or control (C1; normoxic) tanks. Vertical break in the time axis represents the 24 h separation between repeated A1 and A2 or H1 and H2 exposures. Treatment codes as in text. Values are means ± SE from 4–6 individuals per treatment; later samples in A1 treatments lack error bars because only 1 individual maintained its righting reflex at that time.

−18.6; A1+24: −23.3 to −19.3: A1+A2: −20.1 to −17.0), but these did not overlap with the 95% confidence intervals for the slope of either C1+2 (−13.5 to −8.6) or C1+24 (−15.8 to −9.2). A2 could not be included in the Gauss-Newton analysis due to the limited data (only collected to 50 min). These results indicate rapid depression of ventilatory rate (we did not measure ventilatory volume) during anoxia. In contrast to anoxia, ventilation rate remained significantly elevated relative to controls at 50–60 beats/min for the duration of the hypoxia experiments, with no difference between the first and second hypoxic exposures (Fig. 3).

Plasma Lactate Increases Dramatically After Oxygen Limitation, While Plasma Glucose and Electrolytes Remain Largely Unchanged

Plasma lactate concentrations increased significantly after low-oxygen exposure ($P < 0.001$) (Fig. 4). The highest measured plasma lactate concentrations occurred 2 h after return from anoxia to normoxic conditions (A1+2 h), but we do not know how lactate varied during the episodes of oxygen limitation. In all anoxic and hypoxic treatments plasma lactate returned to baseline values by 24 h recovery. There was a significant, but small, effect of treatment on plasma glucose concentrations ($P = 0.013$) (Fig. 4), with the H1+24, H1+H2+24 and Field treatments tending to have less circulating glucose than other treatments. However, the Tukey's HSD post hoc test failed to detect any pair-wise treatment differences. The less conservative Fisher Least Significant Difference post hoc test revealed three statistically homogeneous groups. There was no significant effect of oxygen limitation on plasma osmolality (K-W; $P = 0.410$), sodium concentration (K-W; $P = 0.098$), or chloride concentration (K-W; $P = 0.219$) (Fig. 5, *A* and *B*). Plasma potassium concentration varied among treatments ($P < 0.001$) (Fig. 5*C*), but the changes were minor and not systematically associated with specific low-oxygen conditions.

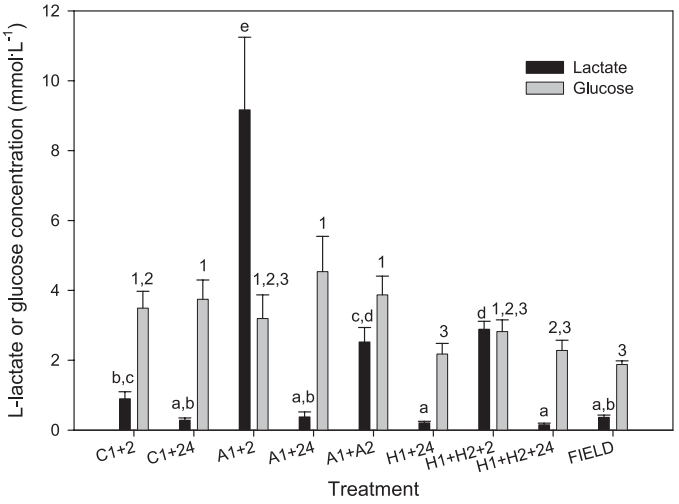

Fig. 4. Plasma lactate and glucose concentrations in epaulette sharks after exposure to control, anoxic, and hypoxic conditions plus recovery (treatment codes as in text). Different lowercase letters represent statistically distinguishable groups for lactate (Tukey's HSD test); numbers represent statistically distinguishable groups for glucose (Fisher's LSD; see text for details). FIELD samples were collected from individuals on the Heron Island reef platform during a nocturnal, spring low tide. Values are means ± SE from 4–6 individuals per treatment.

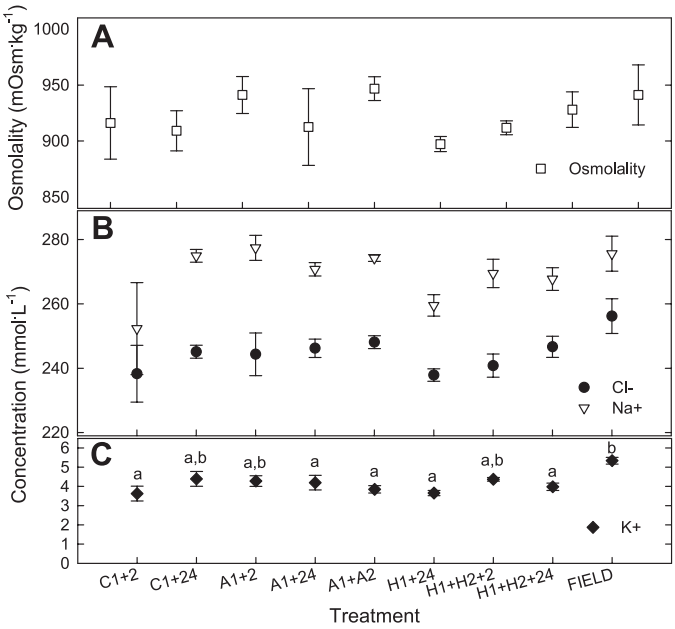

Fig. 5. Epaulette shark plasma. *A*: osmolality, *B*: concentrations of sodium and chloride; *C*: potassium concentration, following exposure to control, anoxic, and hypoxic treatments plus recovery (treatment codes as in text). Different lowercase letters represent statistically distinguishable groups for potassium; there were no significant differences in osmolality, chloride, or sodium. FIELD samples were collected from individuals on the Heron Island reef platform during a nocturnal, spring low tide. Values are means ± SE from 4–6 individuals per treatment.

Ion-Pumping and Apoptotic Effector Enzyme Activities Do Not Respond to Oxygen Limitation and Recovery

There were no differences in cerebellum or rectal gland Na^+/K^+ ATPase activities 24 h after anoxic or hypoxic exposure (Table 1). Rectal gland Na^+/K^+ ATPase activity was significantly greater than that in brain.

There was a significant effect of treatment on caspase 3/7 in brain tissue ($P = 0.032$), but the only pair-wise significant difference detected with the post hoc test was between A1+A2 and H1+24 (Fig. 6*A*). Notably, there were no increases in caspase 3/7 activity in brain following any of the hypoxic or anoxic treatments relative to controls, suggesting no early (2 h) or delayed (24 h) caspase-dependent apoptosis. Similarly, the rectal gland exhibited no increases in caspase 3/7 activity after oxygen limitation (Fig. 6*B*).

No Long-term Effect of Episodic Oxygen Limitation on the Total Glutathione Pool in Cerebellum

There was a significant effect of treatment on both the reduced ($P < 0.001$) and total ($P < 0.001$) glutathione pools in epaulette shark brain (Fig. 7*B*). Specifically, both the control (C1) and anoxia (A1) treatments +2 h exhibited lower levels of both reduced and total glutathione than the corresponding +24 h treatments. A similar, though statistically insignificant, trend was observed for the repeated hypoxia treatments (H1+H2+2 h vs. H1+H2+24 h). The fraction of the total glutathione pool in the reduced state (% GSH) similarly varied among treat-

Table 1. *Activities of Na^+/K^+ ATPase (μmol ADP·h^{-1}·mg protein^{-1}) in epaulette shark rectal gland and brain (cerebellum)*

Tissue	C1 + 24	*n*	A1 + 24	*n*	H1 + 24	*n*	H1+H2+24	*n*
Rectal gland	12.6 ± 2.5	4	12.8 ± 2.2	5	17.8 ± 3.9	6	13.4 ± 2.5	5
Brain	3.9 ± 0.9	4	4.0 ± 0.9	5	3.2 ± 0.1	5	3.6 ± 0.4	6

Values are means ± SE. There were no significant differences among the treatments in either tissue.

ments ($P = 0.003$); more glutathione was oxidized in +2 h brains than in the respective +24 h group for the control (C1), anoxia (A1), and repeated hypoxia (H1+H2) treatments (Fig. 7*A*). These data suggest a common oxidative stressor among the control and experimental treatments, most likely as a result of handling stress when placing the animals in the experimental chambers and removing them after treatment. However, almost all glutathione was in the reduced state (GSH) for the four +24 h treatments (Fig. 7*A*), implying that the GSH system recovered by 24 h regardless of the treatment. Furthermore, there were no significant differences among the four +24 h treatments in the reduced or total glutathione pools.

Small Magnitude, Treatment- and Tissue-Specific Proteome Responses to Episodic Oxygen Limitation and Reoxygenation

Cerebellum. The master gel image for cerebellum contained 986 protein spots that were quantified using Delta 2D software (Supplemental Fig. S1A).[1] Of these, 14 unique spots met the twofold change and 95% confidence criteria in one or more low-oxygen treatments, and the abundances of 75 unique protein spots changed significantly after exposure to anoxia and/or hypoxia using the less stringent criteria (Table 2). Overall, more proteins decreased in relative abundance following low-oxygen exposure than increased. There were also more significant changes in protein abundance in H1+24 h and H1+H2+24 h than in A1+24 h (Table 2). Very few proteins were consistently up- or downregulated in more than one low-oxygen treatment, although 8 proteins were consistently regulated in both H1+24 h and H1+H2+24 h (Table 3). The PLS-DA analysis clearly separated the four treatments based on global expression patterns (Fig. 8*A*), and the reduced PLS-DA model based on the top 49 (5%) VIP scores performed much better than expected by chance (Supplemental Fig. S2A). Sixteen of the top 49 VIP scores (33%) were also selected by the *t*-test/ratio criteria (Table 4).

Of the 108 total cerebellum proteins of interest, 60 (55%) were identified using tandem mass spectrometry combined with bioinformatics searches (Supplemental Table S1). These proteins were placed into a hierarchical functional framework (Table 4) based on IPA/GO annotations and extensive manual review of the relevant literature (see Discussion). These proteins also mapped to a number of canonical cellular pathways in IPA software (Supplemental Table S2). The master molecular interaction network for cerebellum (Supplemental Fig. S3) was created by merging five significantly matching networks in IPA: *1*) carbohydrate metabolism, lipid metabolism, small molecule biochemistry ($P = 10^{-66}$); *2*) gene expression, carbohydrate metabolism, small molecule biochemistry ($P = 10^{-31}$); *3*) neurological disease, skeletal and muscular disorders, behavior ($P = 10^{-10}$); *4*) skeletal and muscular disorders, cell morphology ($P = 0.01$); *5*) neurological disease ($P = 0.01$).

[1] The online version of this article contains supplemental material.

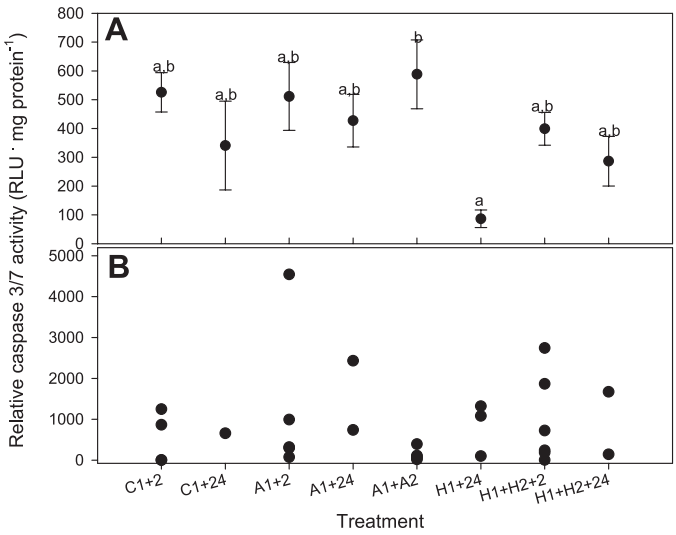

Fig. 6. Combined activity of caspases 3 and 7, two closely related effectors of apoptosis, in epaulette shark brain (cerebellum) (*A*) and rectal gland (*B*) following control (normoxic), anoxic, and hypoxic exposure plus recovery (treatment codes as in text). Activity was determined using a luminescent assay (RLU, relative light units). Different lowercase letters indicate statistically distinguishable groups for brain as determined by Tukey's HSD post hoc test. Values for cerebellum are means ± SE from 4–6 individuals per treatment. Individual data points are presented for rectal gland due to small samples sizes in some treatments.

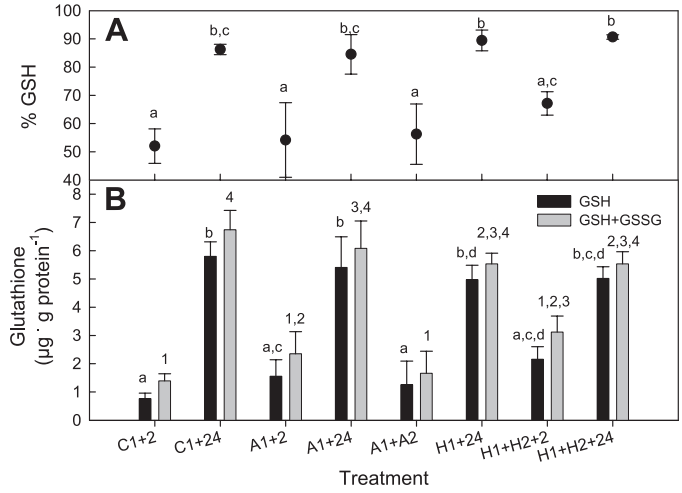

Fig. 7. *A*: percentage of the epaulette shark brain (cerebellum) total glutathione pool in the oxidized form (GSH) following control (normoxic), anoxic, or hypoxic exposure plus recovery (treatment codes as in text). *B*: reduced glutathione (GSH) and total glutathione (GSH+GSSG) pools in epaulette shark cerebellum in each treatment. GSH is oxidized to GSSG during oxidative stress. Different lowercase letters or numbers represent statistically different groups for GSH and total glutathione, respectively. Values are means ± SE from 4–6 individuals per treatment.

Table 2. *Number of significant changes ($P < 0.05$) in relative protein abundance in brain (cerebellum) and rectal gland of epaulette sharks 24 h after exposure to anoxia (A1 + 24) and one (H1 + 24) or two episodes (H1 + H2 + 24) of hypoxia*

	Brain		Rectal Gland	
Treatment	$r < 0.5$ or $r > 2$	$r < 0.67$ or $r > 1.5$	$r < 0.5$ or $r > 2$	$r < 0.67$ or $r > 1.5$
A1 + 24	3 (−), 0 (+)	10 (−), 3 (+)	1 (−), 6 (+)	9 (−), 9 (+)
H1 + 24	6 (−), 1 (+)	25 (−), 14 (+)	6 (−), 19 (+)	33 (−), 48 (+)
H1 + H2 + 24	4 (−), 2 (+)	20 (−), 15 (+)	1 (−), 4 (+)	7 (−), 16 (+)

Values are given for both the strict and lenient expression ratio criteria [r; relative to controls (C1 + 24)]. (+) increased; (−) decreased. Individual protein spots were counted in multiple categories where appropriate.

Rectal gland. The master gel image for rectal gland contained 770 protein spots that were quantified using Delta 2D software (Supplemental Fig. S1B). Of these, 29 unique spots met the twofold change and 95% confidence criteria in one or more low oxygen treatments, and the abundances of 101 unique protein spots changed in response to episodic anoxia and/or hypoxia using the less stringent criteria (Table 2). In contrast to cerebellum, more rectal gland spots were upregulated relative to controls than downregulated. As in cerebellum, the highest number of significant changes in protein abundance occurred in H1+24 h, followed by H1+H2+24 h and then A1+24 h (Table 2). A greater number of consistent changes in individual protein expression occurred across treatments in rectal gland relative to cerebellum (Table 3). The reduced rectal gland PLS-DA model based on the top 38 (5%) VIP scores performed better than expected by chance (Supplemental Fig. S2B) and clearly discriminated among the four treatment groups (Fig. 8*B*). Similar to cerebellum, 14 of the top 38 VIP scores (37%) were also selected by the *t*-test/ratio criteria (Table 5).

Of the 101 proteins of interest in rectal gland, 53 (52%) were identified using tandem mass spectrometry combined with bioinformatics searches (Supplemental Table S3). The significant IPA canonical pathways are presented in Supplemental Table S2. The master molecular interaction network for rectal gland (Supplemental Fig. S4) was created by merging four significantly matching networks in IPA: *1*) energy production, nucleic acid metabolism, small molecule biochemistry ($P = 10^{-30}$); *2*) drug metabolism, lipid metabolism, small molecule biochemistry ($P = 10^{-30}$); *3*) cancer, amino acid metabolism ($P = 10^{-30}$); *4*) unnamed ($P = 0.01$).

The rectal gland and cerebellum interaction networks shared four highly connected protein nodes that may warrant further examination in the context of the molecular response to episodic hypoxia or anoxia in this species (Supplemental Figs. S3 and S4): huntingtin; solute carrier family 2 (facilitated glucose transporter), member 4; hepatocyte nuclear factor 4, alpha; and peroxisome proliferator-activated receptor gamma, coactivator 1 alpha. However, it should be noted that these molecular interaction networks were constructed using data from all three treatment groups (A1+24, H1+24, H1+H2+24), but the response to oxygen limitation varied considerably among treatments.

DISCUSSION

Epaulette Shark as Comparative Model of Hypoxia and Anoxia Tolerance

The epaulette shark offers an appealing comparative system for studying evolutionary and ecological processes leading to "constitutively preconditioned" (66) models of hypoxia and anoxia tolerance as well as hypoxic preconditioning in verte-

Table 3. *Identified proteins with significant ($P < 0.05$) changes in relative expression in more than one low oxygen treatment for both the strict and lenient expression ratio [r; relative to controls (C1 + 24)] criteria*

	Brain		Rectal Gland	
Treatments	$r < 0.5$ or $r > 2$	$r < 0.67$ or $r > 1.5$	$r < 0.5$ or $r > 2$	$r < 0.67$ or $r > 1.5$
A1 + 24, H1 + 24, & H1 + H2 + 24	**0**	**0**	**2**: glyoxalase domain containing 5 (+/+/+)	**2**: glyoxalase domain containing 5 (+/+/+)
H1 + 24 & H1 + H2 + 24	**1**: novel protein (zgc:92871) (*Danio rerio*) (+/+)	**8**: novel protein (zgc:92871) (*Danio rerio*) (+/+); splicing factor, RS rich 5 (−/−); calmodulin (+/+); heat shock 70 kDa protein 4-like (−/−); ubiquitin-conjugating enzyme E2D 2 isoform 1 (+/+); methylcrotonoyl-coenzyme A carboxylase 2 (beta) (−/−)	**4**: glyoxalase domain containing 5 (+/+)	**14**: 14-3-3 epsilon (+/+); glyoxalase domain containing 5 (+/+); 3-oxoacid CoA transferase 1 (−/−); heat shock cognate 70 kDa (−/−); creatine kinase (+/+)
A1 + 24 & H1 + 24	**0**	**3**: EF hand calcium binding protein 2 (−/−)	**3**: peptidylprolyl isomerase B (+/+); glyoxalase domain containing 5 (+/+)	**5**: peptidylprolyl isomerase B (+/+); glyoxalase domain containing 5 (+/+)
A1 + 24 & H1 + H2 + 24	**1**: alpha tubulin (−/−)	**1**: alpha tubulin (−/−)	**3**: glyoxalase domain containing 5 (+/+)	**4**: pyruvate dehydrogenase (lipoamide) beta (−/−); glyoxalase domain containing 5 (+/+)

Bold numbers indicate the total number of commonly regulated proteins; unidentified proteins are included in the tallies (for their expression changes see Supplemental Tables S4 and S5). Signs [(+/+),(+/−), etc.] indicate relative changes in the corresponding treatments.

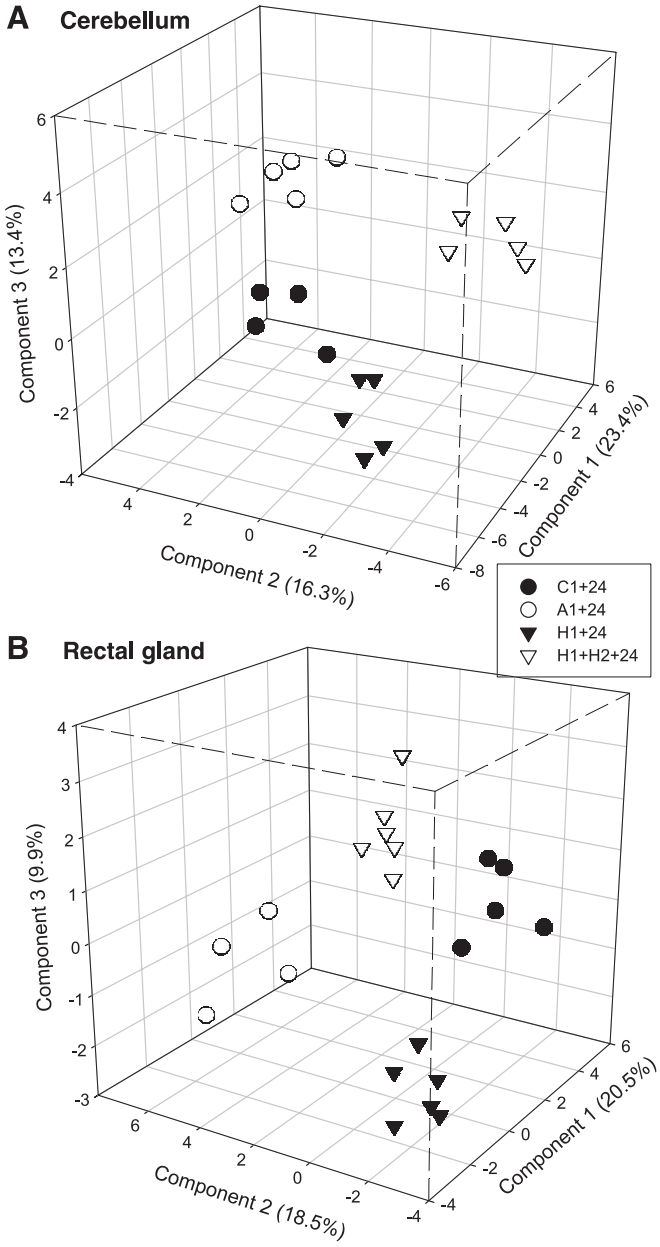

Fig. 8. Three-dimensional PLS-DA score plots for epaulette shark protein expression patterns, based on normalized, mean-centered data. Each data point represents the proteome of 1 individual. *A*: reduced cerebellum PLS-DA model based on the top 5% of VIP scores (49 spots). *B*: reduced rectal gland PLS-DA model based on the top 5% of VIP scores (38 spots). Percentages for each component (axis) represent the proportion of variation in the protein expression dataset explained by that component of the model. Treatment codes as in text.

brates. The duration (2 h) and severity (5% air saturation or complete anoxia) of the experimental regimen used here exceed those that would be tolerable by most naïve mammalian systems. Much previous work on tolerance of oxygen limitation in fishes has involved species from the Teleostei (bony fishes), but few studies have addressed mechanisms of hypoxia or anoxia tolerance in the Chondrichthyes (sharks, skates, rays, and chimaeras). Recent works suggest that a few sharks other than the epaulette periodically enter (39) and/or tolerate (13) severely hypoxic or anoxic waters. Unearthing the mechanisms of hypoxia and anoxia tolerance and preconditioning in this ancestral vertebrate lineage may provide important insights into the evolution of these traits and the relative importance of conserved (e.g., reduced glutamate signaling, 104) vs. unique mechanisms.

Our results indicate a suite of small-magnitude changes for proteins involved in several processes relevant to the survival of oxygen limitation and reoxygenation (31). Notably, the relative importance of these responses in the epaulette shark appears to vary depending on the tissue and treatment examined. While proteome responses to H1 and H2 were more similar to each other than to A1 (Table 3), responses to the four treatments were clearly distinguished in the PLS-DA analysis for each tissue (Fig. 8). Surprisingly, one episode of anoxia elicited fewer changes in protein expression than either one or two episodes of hypoxia. Several of the identified proteins and processes in both cerebellum and rectal gland have highly conserved functions among hypoxia or anoxia-tolerant vertebrates, although these mechanisms remain to be further validated in this species. We discuss several of the more prominent patterns in these two tissues and propose novel hypotheses for both enhanced hypoxia and anoxia tolerance and preconditioning in the epaulette shark.

Prevention of Excitotoxicity in Cerebellum: Decreased Excitatory Neurotransmission, Modified Vesicle Dynamics, and Increased Calcium Binding

A number of protein expression changes in the cerebellum were consistent with the prevention of excitotoxicity via their roles in neurotransmitter dynamics. One of the major causes of neuronal cell death in cerebral ischemia/reperfusion, excitotoxicity involves a cascade of events including elevation of cytosolic calcium concentration ($[Ca^{2+}]_i$), resulting in release of the excitatory neurotransmitter glutamate and initiation of a lethal cycle of membrane depolarization. The classical adaptive decrease in action potential firing, via decreased glutamate signaling, during oxygen limitation in tolerant animals is known as "spike arrest" (97). Several proteins potentially related to glutamate production and release were downregulated in epaulette shark cerebellum following two episodes of hypoxia and, to a lesser extent, anoxia. Foremost among these, the decrease in GLS (all abbreviations as in Tables 4 and 5) after H2 is consistent with reduced glutamate production (45) after multiple hypoxic episodes.

Several of the identified proteins play important roles in vesicle dynamics, implying adjustments in cycling of neurotransmitters and/or receptors in epaulette shark neurons after episodic oxygen limitation. Again, these changes were most pronounced following two hypoxic episodes. The SNAP protein NAPB (↓ A1 and ↓ H2) recruits NSF to membranes for vesicle fusion and exocytosis (i.e., for neurotransmitter release) (100). NSF itself also decreased here after H2, which could have antiexcitotoxic pre- and postsynaptic consequences via decreased glutamate release (77) and decreased stabilization of AMPA glutamate receptors in the postsynaptic membrane (6), respectively. SH3GL1 decreased after A1; this protein may be needed for vesicle fusion in the presynaptic terminal (86). Two additional proteins that may participate in postsynaptic, receptor-mediated endocytosis (CLTA ↓ H1) and trafficking of

Table 4. *Expression ratios (relative to control C1 + 24) for epaulette shark cerebellum proteins regulated by episodic anoxia (A1 + 24) or hypoxia (H1 + 24; H1 + H2 + 24)*

Spot	VIP	VIP Score	Protein Identification	Abbrev.	Expression Ratio A1 + 24	*P*	H1 + 24	*P*	H1 + H2 + 24	*P*
			Energy-producing processes							
Glycolysis										
1.5–66			glyceraldehyde-3-phosphate dehydrogenase (GAPDH) (*Paralichthys olivaceus*)	GAPDH	0.82	0.242	**0.65**	**0.005**	0.69	**0.002**
Oxidative phosphorylation/electron transport chain										
1.5–33	VIP06	1.69	mitochondrial ATP synthase alpha-subunit (*Cyprinus carpio*)	ATP5A1	**0.67**	**0.002**	0.89	0.453	1.24	0.091
1.5–36	VIP08	1.68	ATP synthase subunit alpha (*Larus ridibundus*)	ATP5A1	**0.59**	**0.016**	0.62	0.104	1.16	0.407
1.5–38			mitochondrial ATP synthase, H^+ transporting F1 complex beta subunit (*Mus musculus*)	ATP5B	1.52	0.153	**1.84**	**0.033**	1.15	0.396
	VIP16	1.59	NADH dehydrogenase flavoprotein 2, 24 kDa subunit	NDUFV2	0.89	0.124	0.96	0.572	0.79	**0.025**
Oxidative substrate switching										
1.5–64			3-oxoacid CoA transferase 1 precursor (*Homo sapiens*)	OXCT1	1.25	0.349	**1.65**	**0.012**	1.96	0.061
1.5–26			methylcrotonoyl-Coenzyme A carboxylase 2 (beta) (*Homo sapiens*)	MCCC2	1.04	0.772	**0.66**	**0.015**	**0.63**	**0.016**
1.5–31			propionyl-CoA carboxylase (*Xenopus laevis*)	PCCA	1.27	0.346	1.76	0.089	**1.60**	**0.007**
Intracellular movement of energetic equivalents										
	VIP04	1.73	voltage-dependent anion-selective channel protein 2 (*Xenopus laevis*)	VDAC2	1.06	0.672	1.24	0.085	0.76	**0.046**
	VIP23	1.56	voltage-dependent anion-selective channel protein 2 (*Squalus acanthias*)	VDAC2	0.76	**0.021**	0.71	**0.013**	0.86	0.202
			Energy-consuming processes							
Proteolysis in proteasome										
1.5–39			proteasome 26S ATPase subunit 2 (*Homo sapiens*)	PSMC2	0.91	0.367	**0.62**	**0.030**	0.84	**0.027**
1.5–40	VIP19	1.56	proteasome 26S non-ATPase subunit 11	PSMD11	0.86	0.113	0.83	0.213	**0.55**	**0.002**
Lysosome										
1.5–29			H+-ATPase beta 1 subunit, lysosomal	ATP6V1B1	1.03	0.801	1.46	**0.013**	**1.90**	**0.015**
Transcription and mRNA processing										
2–7			splicing factor, arginine/serine-rich 5a (*Danio rerio*)	SFRS5	0.82	0.366	**0.45**	**0.001**	**0.63**	**0.008**
1.5–62			RNA binding motif protein 8A (*Danio rerio*)	RBM8A	0.78	0.264	0.76	0.289	**0.60**	**0.047**
Translation										
1.5–30			seryl tRNA synthetase (*Danio rerio*)	SARS	0.73	0.156	0.70	0.085	**0.65**	**0.040**
1.5–48			acidic ribosomal phosphoprotein PO (*Bos taurus*)	RPLP0	0.95	0.713	**0.63**	**0.038**	1.03	0.887
	VIP43	1.48	elongation factor 1-delta (*Tetraodon nigroviridis*)	EEF1D	0.71	0.210	0.95	0.811	0.55	0.080
			Apoptosis and cell cycle							
1.5–14			far upstream element-binding protein (*Homo sapiens*)	FUBP1	1.26	0.367	1.48	0.195	**1.95**	**0.024**
1.5–23	VIP28	1.53	ubiquitin-conjugating enzyme E2D 2 isoform 1 (*Homo sapiens*)	UBE2D2	0.64	0.075	**1.59**	**0.027**	**1.55**	**0.031**
1.5–45			protein phosphatase 1 alpha (*Danio rerio*)	PPP1CA	1.10	0.649	**0.64**	**0.017**	0.66	0.060
1.5–58			Ras-related nuclear protein (*Ictalurus punctatus*)	RAN	1.14	0.355	**1.57**	**0.041**	1.37	0.091
	VIP26	1.54	high mobility group box 2 (*Mus musculus*)	HMGB2	0.58	0.071	0.76	0.271	0.69	0.184

Continued

Table 4.—*Continued*

Spot	VIP	VIP Score	Protein Identification	Abbrev.	Expression Ratio A1 + 24	*P*	H1 + 24	*P*	H1 + H2 + 24	*P*
			Neurotransmitters							
Glutamate synthesis/degradation										
1.5–27			glutaminase (*Rattus norvegicus*)	GLS	0.78	0.223	1.00	0.998	**0.53**	**0.004**
Receptor processing, vesicle fusion (exo- and endocytosis)										
1.5–15			N-ethylmaleimide sensitive fusion protein (*Cricetulus longicaudatus*)	NSF	0.80	0.272	0.70	0.140	**0.66**	**0.033**
	VIP01	1.92	N-ethylmaleimide sensitive fusion protein attachment protein beta (*Mus musculus*)	NAPB	0.70	**0.004**	0.82	0.101	0.78	**0.021**
1.5–44			SH3 domain-containing Grb-2-like protein (*Xenopus tropicalis*)	SH3GL1	**0.60**	**0.041**	0.87	0.491	0.77	0.449
1.5–51	VIP09	1.67	clathrin light-chain B isoform 1 (*Monodelphis domestica*)	CLTA	0.73	0.052	**0.61**	**0.011**	0.78	0.115
	VIP34	1.51	dihydropyrimidinase-like 2 (*Danio rerio*)/collapsin response mediator protein-1A	DPYSL2	1.11	**0.046**	0.97	0.562	0.91	0.075
1.5–52			toll interacting protein (*Xenopus tropicalis*)	TOLLIP	1.04	0.829	**0.57**	**0.011**	0.73	0.065
			Ca^{2+} binding							
2–14			novel protein similar to vertebrate EF hand calcium binding protein 2 (*Danio rerio*)	NECAB2	**0.65**	**0.029**	**0.36**	**0.001**	0.54	0.205
1.5–18	VIP31	1.52	calmodulin (*Clemmys japonica*)	CALM1	0.80	0.187	**1.83**	**0.018**	**1.60**	**0.003**
			Molecular chaperones							
1.5–20			heat shock 70 kDa protein 4-like (unnamed protein product, *Tetraodon nigroviridis*)	HSPA4L	0.87	0.424	**0.60**	**0.021**	**0.61**	**0.022**
	VIP03	1.74	chain A, dimerizaton and U-box domains of zebrafish c-terminal of HSP70 interacting protein	HSPBP1	0.97	0.723	1.15	0.095	0.69	0.062
1.5–56			prohibitin (*Equus caballus*)	PHB	0.80	0.603	0.94	0.864	**1.63**	**0.036**
			Cytoskeleton							
Microtubular skeleton										
2–4	VIP47	1.47	alpha tubulin (*Gillichthys mirabilis*)	TUBA1A	**0.32**	**0.001**	0.52	0.158	0.55	0.150
2–5			alpha tubulin (*Gillichthys mirabilis*)	TUBA1A	**0.34**	**0.016**	0.73	0.703	**0.22**	**0.014**
1.5–12			alpha tubulin	TUBA1A	1.36	0.133	1.47	**0.018**	**1.70**	**0.034**
1.5–13	VIP27	1.54	alpha tubulin subunit (*Oncorhynchus nerka*)	TUBA1A	1.11	0.494	1.12	0.277	**1.52**	**0.002**
1.5–28			alpha tubulin	TUBA1A	**1.51**	**0.024**	1.69	0.280	1.20	0.384
1.5–32			alpha tubulin	TUBA1A	1.13	0.664	**1.55**	**0.037**	1.49	0.187
1.5–34			alpha tubulin	TUBA1A	1.31	0.211	**1.60**	**0.005**	1.26	0.265
1.5–70			tubulin alpha	TUBA1A	1.05	0.888	**1.97**	**0.045**	2.61	0.059
1.5–50			alpha 4 tubulin	TUBA4A	1.21	0.184	**0.57**	**0.017**	0.64	0.081
2–9			tubulin folding cofactor B (cytoskeleton-associated protein 1) (LOC735205, *Xenopus laevis*)	TBCB	0.63	0.152	**0.30**	**0.002**	0.68	0.233
Actin cytoskeleton and dendrite morphology										
1.5–42			beta actin	ACTB	1.03	0.936	2.10	0.107	**1.87**	**0.048**
1.5–11			marcks (myristoylated alanine-rich C-kinase substrate) calmodulin binding domain protein	MARCKS	0.76	0.152	1.09	0.778	**0.62**	**0.034**
1.5–10			dynamin 3	DNM3	0.73	0.110	0.70	**0.029**	**0.61**	**0.011**
Intermediate filaments										
1.5–41			glial fibrillary acidic protein (*Mus musculus*)	GFAP	1.06	0.799	**1.73**	**0.013**	1.38	0.136

Continued

Table 4.—*Continued*

Spot	VIP	VIP Score	Protein Identification	Abbrev.	Expression Ratio A1 + 24	*P*	H1 + 24	*P*	H1 + H2 + 24	*P*
Cytoskeleton anchoring										
1.5–25	VIP35	1.51	ezrin	EZR	0.91	0.603	**1.56**	**0.028**	1.12	0.388
1.5–54			nebulette (*Homo sapiens*)	NEBL	1.04	0.779	0.77	0.232	**0.63**	**0.033**
1.5–43			ribosomal protein SA (laminin-binding protein) (*Homo sapiens*)	RPSA	0.99	0.959	**0.51**	**0.021**	0.69	0.086
			Signaling pathways							
cAMP-dependent protein kinase (PKA)										
2–6			cAMP-dependent protein kinase type II-beta regulatory subunit isoform 1 (*Canis familiaris*)	PRKAR2B	1.10	0.774	**0.42**	**0.047**	0.95	0.907
1.5–37			cAMP-dependent protein kinase type I-alpha regulatory subunit (*Mus musculus*)	PRKAR1A	0.92	0.428	1.56	0.151	**1.68**	**0.007**
14-3-3 mediated phophoprotein adapter signaling										
1.5–55	VIP15	1.60	14-3-3 theta (*Danio rerio*)	YWHAQ	0.62	0.097	**0.54**	**0.049**	0.82	0.373
	VIP21	1.56	3-monooxygenase/tryptophan 5-monooxygenase activation protein, gamma polypeptide (14-3-3 gamma) (*Danio rerio*)	YWHAG	0.89	**0.033**	1.02	0.696	0.94	0.273
	VIP46	1.47	14-3-3 beta (*Tetraodon nigroviridis*)	YWHAB	0.75	**0.030**	0.77	0.068	0.83	0.136
G protein-coupled receptors										
1.5–47			guanine nucleotide binding protein G(o), alpha subunit (*Salmo salar*)	GNAO1	0.91	0.709	**0.59**	**0.007**	0.82	0.416
			ROS/oxidative stress							
1.5–35			aldehyde dehydrogenase 7 family, member A1 (*Monodelphis domestica*)	ALDH7A1	0.82	0.252	0.82	0.399	**0.63**	**0.040**
			Unannotated							
2–2	VIP29	1.53	novel protein (zgc:92871) (*Danio rerio*)		0.67	0.504	**2.93**	**0.005**	**2.26**	**0.029**

Proteins were grouped by putative function based on Gene Ontology annotations and manual review of the literature. Values in boldface met the statistical ($P < 0.05$) and expression ratio (<0.67 or >1.5) criteria for mass spectrometry analysis in that treatment. Variable importance in the projection ranks (VIP) and scores (VIP score) based on a partial least squares discriminant analysis are also presented. Expression data for unidentified protein spots can be found in Supplemental Table S4.

ubiquinated endosome-contained proteins such as receptors (TOLLIP ↓ H1) decreased significantly after only one episode of hypoxia, but the significance of these expression changes is unknown. Meanwhile, the lysosomal H^+-ATPase ATP6V1B1 increased after both H1 and H2, possibly indicating activation of lysosomal degradation pathways following hypoxia.

Two calcium-binding proteins were also regulated by hypoxic or anoxic exposure in brain. Expression of the EF-hand domain-containing protein NECAB2 (↓ A1 and H1) is inversely correlated with cell surface expression of adenosine A_2A receptors (11). Our result implies increased availability of A_2A receptors following anoxia or hypoxia, consistent with the role for adenosine in the epaulette shark's response to oxygen limitation (71, 85). Binding of adenosine to the A_2A receptor in mammalian models increases $[Ca^{2+}]_i$; accordingly, we observed that CALM increased after both H1 and H2. This suggests enhanced Ca^{2+} binding capacity to prevent excitotoxicity and/or elevated calmodulin-dependent signaling, the latter of which plays a known role in the cellular response to hypoxia (95). Overall, our results imply that modulation of the controls of $[Ca^{2+}]_i$ and excitotoxicity plays an important role in the epaulette shark cerebellum's response to episodic oxygen limitation.

Cytoskeletal and Membrane Rearrangements in Response to Hypoxia

Another prominent result from the cerebellum was the proteomic evidence for cytoskeletal and membrane reorganization following oxygen limitation, particularly after two episodes of hypoxia (H2). Nine protein spots identified as alpha tubulins exhibited significant expression changes in cerebellum following hypoxia (4 after H1, 3 after H2), and the tubulin folding cofactor TBCB decreased after H1, suggesting remodeling of microtubule networks. We also observed changes in the abundance of an actin cytoskeleton component (ACTB ↑ H2), anchoring proteins that link the actin cytoskeleton to the cell

Table 5. *Expression ratios (relative to control C1 + 24) for epaulette shark rectal gland proteins regulated by episodic anoxia (A1 + 24) or hypoxia (H1 + 24; H1 + H2 + 24)*

Spot	VIP	VIP Score	Protein Identification	Abbrev.	Expression Ratio					
					A1 + 24	*P*	H1 + 24	*P*	H1 + H2 + 24	*P*
			Energy-producing processes							
Glycolysis										
	VIP22	1.46	aldolase B (*Equus caballus*)	ALDOB	1.30	0.070	1.30	0.076	0.95	0.702
	VIP11	1.57	triose phosphate isomerase (*Xiphophorus maculatus*)	TPI1	0.72	**0.010**	0.85	0.159	0.77	**0.012**
1.5–47			glyceraldehyde-3-phosphate dehydrogenase (*Paralichthys olivaceus*)	GAPDH	**1.72**	**0.024**	1.46	0.171	1.36	0.213
1.5–60			phosphoglycerate mutase 1 (*Gallus gallus*)	PGAM1	**0.62**	**0.014**	0.87	0.553	0.77	0.299
Pyruvate dehydrogenase complex										
2–12	VIP13	1.54	pyruvate dehydrogenase (lipoamide) beta (*Danio rerio*)	PDHB	**2.08**	**0.023**	1.06	0.862	**1.95**	**0.007**
1.5–48	VIP17	1.51	pyruvate dehydrogenase (lipoamide) beta (*Danio rerio*)	PDHB	**1.55**	**0.031**	1.10	0.633	1.45	**0.029**
1.5–28			dihydrolipoamide branched chain transacylase E2 (*Taeniopygia guttata)*	DBT	1.34	0.260	2.86	0.202	**1.85**	**0.015**
TCA cycle										
2–14			isocitrate dehydrogenase 2 (NADP+), mitochondrial	IDH2	0.80	0.386	**2.57**	**0.030**	1.43	0.266
Oxidative phosphorylation/electron transport chain										
2–6			ATP synthase subunit alpha, mitochondrial precursor (*Salmo salar*)	ATP5A1	0.64	0.253	**0.37**	**0.047**	0.49	0.133
1.5–27			mitochondrial ATP synthase alpha subunit (*Scyliorhinus canicula*)	ATP5A1	**0.56**	**0.024**	1.04	0.866	1.37	0.164
	VIP23	1.44	ATP synthase, H^+ transporting, mitochondrial F1 complex, alpha subunit (*Danio rerio*)	ATP5A1	0.81	0.121	0.89	0.326	0.85	0.255
1.5–10			NADH dehydrogenase (ubiquinone) Fe-S protein 1 (*Danio rerio*)	NDUFS1	0.88	0.478	**0.51**	**0.001**	0.80	0.259
1.5–11			NADH dehydrogenase (ubiquinone) Fe-S protein 1, 75 kDa (NADH-coenzyme Q reductase) (*Gallus gallus*)	NDUFS1	0.94	0.667	**0.64**	**0.008**	0.84	0.227
1.5–14			NADH dehydrogenase (ubiquinone) Fe-S protein 1, 75 kDa (NADH-coenzyme Q reductase) (*Gallus gallus*)	NDUFS1	0.99	0.963	**0.67**	**0.012**	0.97	0.857
1.5–54	VIP10	1.57	similar to NADH dehydrogenase (ubiquinone) Fe-S protein 3, 30 kDa (NADH-coenzyme Q reductase)	NDUFS3	**0.61**	**0.024**	0.85	0.253	0.77	0.096
1.5–55			succinate dehydrogenase complex, subunit B, iron sulfur (Ip) (*Danio rerio*)	SDHB	0.99	0.941	**0.57**	**0.005**	0.74	0.058
Intracellular movement of energetic equivalents (Malate aspartate shuttle, phosphocreatine circuit)										
1.5–35			mitochondrial aspartate aminotransferase	GOT2	**1.57**	**0.047**	1.23	0.456	1.16	0.459
1.5–52	VIP02	1.67	voltage-dependent anion channel 2 (*Squalus acanthias*)	VDAC2	**0.50**	**0.005**	0.92	0.589	0.85	0.218
1.5–37			creatine kinase (*Scyliorhinus canicula*)	CKB	1.15	0.496	**1.57**	**0.046**	1.28	0.171
1.5–41			creatine kinase (*Scyliorhinus canicula*)	CKB	0.96	0.883	**1.77**	**0.003**	**1.56**	**0.040**

Continued

Table 5.—*Continued*

Spot	VIP	VIP Score	Protein Identification	Abbrev.	Expression Ratio A1 + 24	*P*	H1 + 24	*P*	H1 + H2 + 24	*P*
Oxidative substrate switching										
1.5–24	VIP38	1.39	3-oxoacid CoA transferase (oxct1) (*Xenopus tropicalis*)	OXCT1	0.98	0.905	**0.61**	**0.002**	**0.58**	**0.000**
	VIP37	1.40	3-hydroxyacyl-CoA dehydrogenase	HADH	0.82	0.100	1.00	0.986	0.88	0.315
2–11			acyl-CoA dehydrogenase (EC 1.3.99.3) precursor, short-chain-specific	ACADS	0.90	0.859	**2.83**	**0.006**	1.86	0.058
			Energy-consuming processes							
Proteolysis										
1.5–53			ubiquitin carboxyl-terminal esterase L3 (thioesterase)	UCHL3	1.24	0.190	**1.54**	**0.032**	1.39	0.143
			Apoptosis and cell cycle							
	VIP07	1.60	similar to Cytidylate kinase (UMP-CMP kinase), partial (*Ornithorhynchus anatinus*)	CMPK1	1.03	0.659	1.00	0.970	1.14	0.148
	VIP05	1.63	annexin VII	ANXA7	1.36	**0.047**	0.91	0.413	0.73	0.101
			Vesicles, endocytosis, intracellular trafficking							
1.5–58			RAB37, member RAS oncogene family (*Homo sapiens*)	RAB37	0.69	0.195	**0.60**	**0.049**	0.84	0.447
2–16	VIP29	1.42	glioblastoma amplified sequence (NipSnap2)	GBAS	**2.84**	**0.030**	2.08	0.070	1.51	0.374
	VIP27	1.42	sorting nexin 4 (*Homo sapiens*)	SNX4	1.51	0.115	0.86	0.323	1.07	0.657
			Molecular chaperones							
2–17			peptidylprolyl isomerase B (*Danio rerio*)	PPIB	**2.54**	**0.045**	**2.79**	**0.014**	2.04	0.093
1.5–18	VIP26	1.43	heat shock 70 kDa protein 9B (75 kDa glucose-regulated protein) (*Gallus gallus*)	HSPA9	0.76	**0.024**	**0.66**	**0.004**	0.76	**0.030**
1.5–19			heat shock cognate 70 kDa (*Carassius auratus*)	HSPA8	0.87	0.386	**0.66**	**0.004**	**0.58**	**0.037**
1.5–40			DnaJ (Hsp40) homolog, subfamily B, member 11 (*Homo sapiens*)	DNAJB11	1.03	0.920	**1.96**	**0.036**	1.44	0.165
			Cytoskeleton							
Microtubular skeleton										
	VIP14	1.54	tubulin beta-1 chain (*Gadus morhua*)	TUBB1	0.89	0.243	1.03	0.809	1.34	**0.002**
Actin cytoskeleton										
2–26			tropomyosin (*Takifugu rubripes*)	TPM1	1.55	0.222	**2.61**	**0.029**	2.14	0.112
1.5–43			fast tropomyosin (*Scyliorhinus retifer*)	TPM1	1.11	0.675	**1.83**	**0.024**	1.54	0.156
1.5–49			cytoskeletal tropomyosin 4 (*Coturnix coturnix*)	TPM4	1.17	0.473	**1.79**	**0.047**	1.72	0.096
1.5–36			tropomodulin 2 (*Danio rerio*)	TMOD2	1.23	0.600	**1.54**	**0.036**	1.25	0.477
Intermediate filaments										
1.5–34			type II keratin K8 (*Scyliorhinus stellaris*)	KRT8	0.99	0.939	**1.66**	**0.024**	1.31	**0.050**
Cytoskeleton anchoring										
1.5–9			radixin	RDX	0.98	0.907	**0.63**	**0.035**	0.90	0.613
1.5–12			moesin/radixin	MSN	1.06	0.738	**0.65**	**0.028**	0.93	0.776
1.5–13			similar to Moesin (membrane-organizing extension spike protein)	MSN	1.02	0.869	**0.63**	**0.029**	0.97	0.839
Mitochondrial cristae structure										
1.5–6			mitofilin (mitochondrial inner membrane protein) (*Homo sapiens*)	IMMT	1.11	0.622	**0.55**	**0.005**	1.02	0.908

Continued

Table 5.—*Continued*

Spot	VIP	VIP Score	Protein Identification	Abbrev.	Expression Ratio A1 + 24	*P*	H1 + 24	*P*	H1 + H2 + 24	*P*
			Signaling pathways							
cAMP-dependent protein kinase (PKA)										
1.5–31			cAMP-dependent protein kinase, regulatory subunit alpha 1 (*Homo sapiens*)	PRKAR1A	1.18	0.631	**0.62**	**0.033**	0.89	0.551
14-3-3 mediated phophoprotein adapter signaling										
2–15			14-3-3 epsilon	YWHAE	1.51	0.079	**2.41**	**0.002**	**1.96**	**0.009**
1.5–51			14-3-3 epsilon (tyrosine 3/tryptophan 5 - monooxygenase activation protein, epsilon polypeptide)	YWHAE	0.99	0.953	**1.54**	**0.035**	1.38	0.144
Oxygen sensing										
	VIP25	1.43	cystathionase (*Danio rerio*)	CTH	1.10	0.416	1.13	0.228	1.43	**0.012**
			ROS/oxidative stress							
2–21	VIP01	2.02	glyoxalase domain containing 5	GLOD5	**4.28**	**0.001**	**3.39**	**0.001**	**2.86**	**0.005**
1.5–23			aldehyde dehydrogenase 4 family, member A1 (*Danio rerio*)	ALDH4A1	1.04	0.868	**1.54**	**0.019**	1.39	0.070
1.5–26			aldehyde dehydrogenase 7 family, member A1	ALDH7A1	0.67	0.175	0.68	0.229	**0.52**	**0.015**
1.5–71			ferritin, heavy polypeptide	FTH1	1.34	0.415	**1.73**	**0.023**	1.44	0.171
1.5–64			Parkinson disease 7 (DJ-1)	PARK7	1.20	0.610	**1.85**	**0.049**	1.67	0.234
	VIP20	1.47	ubiquinone biosynthesis methyltransferase COQ5 (unnamed protein product, *Tetraodon nigroviridis*)	COQ5	1.34	0.093	1.24	**0.020**	1.31	**0.004**

Proteins were grouped by putative function based on Gene Ontology annotations and manual review of the literature. All columns as in Table 4. Expression data for unidentified protein spots can be found in Supplemental Table S5.

membrane (EZR ↑ H1) or to the extracellular matrix at focal adhesions (NEBL ↓ H2, 27), and an actin stabilizer (MARCKS ↓ H2). The latter is of particular interest here, because proteasomal degradation of actin-stabilizing MARCKS is involved in transient, translation-independent preconditioning in cultured neurons. This short-term effect was linked to a decrease in the number of postsynaptic dendritic spines, decreased NMDA-type glutamate receptor availability, and decreased glutamate/NMDA excitotoxicity (65). In accord with this mechanism, we also observed decreases in the membrane-associated GTPase DNM3 after both H1 and H2. Recent work demonstrated that DNM3 associates with metabotropic glutamate receptors in postsynaptic dendritic spine tips, and, more importantly, that changes in DNM3 expression lead to remodeling of dendritic spine morphology, possibly via interactions with the actin cytoskeleton (25). Morphological changes in dendrites (a.k.a., synaptic structural plasticity) are known to be involved in memory and learning (29), and they contribute to dynamic and reversible responses of neurons to stimuli (69, 72).

On the basis of our data, we hypothesize that an analogous mechanism of dendrite spine retraction contributes to prolonged excitotoxicity prevention following hypoxic exposure (especially after H2, but not anoxia) in the epaulette shark cerebellum. Because the density of dendritic spines is positively correlated with the availability of AMPA glutamate receptors (73), such structural plasticity would represent a potentially powerful preconditioning mechanism for enhanced damage prevention following repeated hypoxia in the epaulette shark brain. Further work is needed to clarify its significance in this context.

The evidence for cytoskeletal and membrane changes in response to hypoxia was not limited to the cerebellum. The rectal gland exhibited upregulation after H1 of three spots identified as tropomyosins, as well as TMOD2. Together, these proteins regulate the interaction of actin and myosin as well as the length of actin filaments. Three proteins from the ezrin/radixin/moesin family of membrane-actin cytoskeletal cross-linkers exhibited the opposite expression pattern compared with the tropomyosins, decreasing after H1 but returning to control levels after H2. Together, these results may indicate transient reorganization of rectal gland cytoskeletal components after one episode of hypoxia. A recent study demonstrated rapid morphological changes at both the tissue and cellular levels following feeding in the dogfish rectal gland (63), and we hypothesize that analogous mechanisms contribute to the epaulette shark rectal gland's response to oxygen limitation here.

Other proteins whose expression changed in the rectal gland were placed in the "vesicles, endocytosis, and intracellular trafficking" category and play putative roles in membrane dynamics as well. However, the implications for membrane plasticity are less clear in this tissue. GBAS (a.k.a. nipsnap2; ↑ A1) belongs to a protein family implicated in vesicular transport (8), although its closest relative nipsnap1 also associates with the inner mitochondrial membrane and perhaps the electron transport chain

(14). Similarly, transient downregulation of IMMT after H1 may indicate mitochondrial cristae structural reorganization and could have implications for metabolite (ADP) flux (38, 121). The function of RAB37 (↓ H1), a GTPase associated with secretory granules in pancreatic beta cells (7), is also unknown in this context.

Greater Efficiency in Metabolic Coupling Rather Than Decreased Capacity

Evidence for a decrease in aerobic or anaerobic energy production capacity, one aspect of canonical metabolic depression, was limited in the present study. The data for plasma lactate levels suggest an organismal shift to anaerobic ATP production, particularly during anoxia, consistent with a continued need for cellular energy supply in the absence of oxygen. Circulating lactate at A1+2 h increased >10-fold over control (C1+2 h) levels; epaulette shark plasma lactate also peaked at anoxia +2 h in a previous study (13). If sustained throughout anaerobic episodes, this increase could compensate for much of the 10- to 18-fold loss of efficiency when relying solely on anaerobic compared with aerobic glucose metabolism (33). Because there was no A1+A2+2 h treatment (A1+A2 lactate increased ~3-fold over C1+2 h), we could not determine whether the response to a second anoxic episode involved a compensatory decrease in organismal lactate production. While both brain and rectal gland exhibited some proteome adjustments consistent with changes in glycolytic flux after oxygen limitation, these responses were not consistent. Importantly, the proteomic and metabolic responses to anoxia in other tissues that constitute a greater fraction of the organismal metabolic rate remain to be investigated.

Interestingly, the proteomic data for rectal gland indicate adjustments that could increase the efficiency of shuttling of pyruvate, the end product of cytosolic glycolysis, to the mitochondria, facilitating its complete oxidation via the tricarboxylic acid (TCA) cycle and electron transport chain (ETC). Two spots identified as PDHB (E1 of the pyruvate dehydrogenase complex) increased significantly after both A1 and H2 in rectal gland, and a third component of the complex (DBT, the E2 catalytic center) also increased after H2. We have no concrete explanation for these results, but it is tempting to speculate that enhanced PDH complex activity would tightly couple cytosolic pyruvate production to mitochondrial oxidative phosphorylation when oxygen is limiting but still available (i.e., during hypoxia). Such tight coupling could also help to prevent buildup of H^+ ions from net ATP hydrolysis during conditions when oxygen is limiting (32). It should also enhance aerobic metabolic efficiency in the gland during the reoxygenation period following anoxia. No analogous changes in the pyruvate dehydrogenase complex were noted in brain.

While our data offer little evidence for systematic changes in anaerobic metabolism following oxygen limitation, previous work in this species clearly demonstrated a decrease in the normoxic aerobic metabolic rate after exposure to multiple hypoxic episodes (89). This result implies decreased flux through the TCA cycle and/or the ETC, where oxygen serves as the terminal electron acceptor. Our data indicate only minimal adjustments in the TCA cycle for the tissues examined, while the patterns for the ETC are again tissue- and treatment-specific. No TCA enzymes changed abundance following any treatment in cerebellum. In the ETC, two spots identified as ATP5A1 (ETC complex V) decreased after anoxia, possibly indicating reduced oxidative phosphorylation capacity. ATP5B increased after H1 in cerebellum, while NDUFV2 (ETC complex I) decreased after H2. ATP5B contains the catalytic site of ATP synthase (complex V), possibly indicating a more efficient coupling of ATP synthesis to the H^+ ion gradient across the inner mitochondrial membrane after one episode of hypoxia (analogous to the PDHB argument in rectal gland above). Notably, expression of ATP5B also increased in two chemical preconditioning models (1, 90) and after hepatic ischemic preconditioning in mouse, where it was proposed to offer protection from reperfusion injury (118). In rectal gland, the only observed changes in TCA cycle enzymes were an increase in IDH2 after H1 (see below) and a decrease in SDHB (also a component of ETC complex II) after H1. Other ETC proteins in complex I (NDUFS1, NDUFS3) and complex V (ATP5A1) were also downregulated to varying degrees after A1 or H1, but generally not after H2. It is possible that the organismal decreases in aerobic metabolic rate observed in Ref. 89 reflect the contributions of other tissues and/or require more than two episodes of hypoxia to take effect.

Although the proteomic results for aerobic metabolic pathways in the tissues examined are somewhat ambiguous, the organismal response to repeated episodes of hypoxia reflected continued reliance on oxidative metabolism; there was no evidence for decreased ventilatory rate during H2 compared with H1. In addition, epaulette shark hemoglobin appears to have a high affinity for oxygen, and the critical oxygen tension further decreases after preexposure to hypoxia (89). These results suggest that physiological responses to hypoxia in this species work to maintain oxygen delivery to the tissues during successive hypoxic episodes, rather than depressing aerobic metabolism. Notably, lactate levels still increased more than threefold at H1+H2+2 h relative to C1+2 h. This indicates that anaerobic pathways must be invoked to supplement aerobic ATP production during hypoxia, allowing epaulette sharks to sustain metabolic activity under these conditions.

Limited Evidence for Decreased Energy Demand

Reduced energy demand is the other hallmark of species that survive prolonged oxygen limitation by invoking metabolic depression, but, as for energy production, our data provide inconclusive evidence for a decrease in energy-consuming processes following episodic oxygen limitation. Transcription and translation (i.e., protein synthesis) account for a large fraction of the cellular energy budget (88). Several proteins involved in these functions were significantly downregulated in brain following hypoxia, but not anoxia. SFRS5 (↓ H1 and H2) participates in mRNA splicing, as does RBM8A (↓ H2) (94). The opposite pattern of SFRS5 expression appeared in ischemic mouse brain (93). The tRNA transporter SARS (↓ H2) and the 60S ribosome subunit RPLP0 (↓ H1) are necessary for (ATP-dependent) translation at the ribosome. Although these results may be consistent with decreased protein synthesis in brain following hypoxia and recovery, these proteins represent only a small fraction of the large complexes that carry out transcription and translation. We found no evidence

for suppression of these two processes in the rectal gland following any of the treatments.

Other proteins involved in protein degradation via the proteasome decreased in cerebellum following one or more episodes of hypoxia and reoxygenation, possibly indicating reduced protein turnover in this tissue (49). PSMC2 (↓ H1 and H2) forms part of the 19S regulatory proteasome cap, where it unfolds and deubiquitinates proteins prior to their degradation. The 19S proteasome lid component PSMD11 (↓ H2) plays a critical role in assembly and stabilization of the entire 26S proteasome as well as possibly in its substrate specificity (35, 92). Whether these expression changes are sufficient to globally or selectively suppress proteasome-dependent proteolysis remains to be determined. In rectal gland, no proteasome constituents were regulated by oxygen limitation.

Ion pumping represents another energetically costly process for cells, particularly in the brain and rectal gland. Our data provide no evidence for a preconditioning effect on the major monovalent cation-pumping protein Na^+/K^+-ATPase in either tissue. We interpret this finding as evidence for the critical cellular and organismal need to maintain ionic homeostasis and membrane polarity during episodic oxygen limitation (112) and, equally as important, during reoxygenation. Accordingly, our plasma electrolyte data reveal no pervasive loss of ionic homeostasis following any treatment (at +2 h or +24 h). However, we cannot rule out posttranslational control of Na^+/K^+-ATPase during the episodes of oxygen limitation (3, 61).

Substrate Switching and More Efficient Energetic Shuttling to Support Continued Metabolic Activity

The proteome responses following episodic hypoxia, but not anoxia, revealed divergent patterns of substrate utilization for sustained ATP production in cerebellum and rectal gland. The glycolytic enzyme GAPDH, which either increases (30) or is used as a housekeeping gene (91) in mammalian brain ischemia models, decreased in epaulette shark cerebellum after both H1 and H2, possibly indicating a decreased reliance on glucose metabolism. Our data for cerebellum suggest a compensatory increase in ketone body catabolism after hypoxia (OXCT1 ↑ H1), while the decrease in MCCC2 (↓ H1 and H2) implies decreased reliance on branched-chain amino acid catabolism (especially leucine). Ketone bodies, including β-hydroxybutyrate, are a favored substrate in the brain and in elasmobranch tissues in general (2, 16). In contrast, the rectal gland exhibited decreased abundance of OXCT1 after H1 and H2, implying decreased reliance on ketone bodies in this tissue. The rectal gland was recently demonstrated to rely heavily on glucose as a substrate, while β-hydroxybutyrate could only supplement glucose-fueled salt secretion (110). Interestingly, both tissues exhibited an increase in enzymes related to fatty acid metabolism following hypoxia, but not anoxia (odd chain fatty acids: PCCA ↑ H2 in brain; short-chain fatty acids: ACADS ↑ H1 and ↑ H2 in rectal gland). Although fatty acids are not considered an important fuel in elasmobranchs (2), their use may supplement ATP production at critical times. It will be informative to measure circulating and cellular levels of these alternative fuels in the epaulette shark in this context.

Another prominent feature in rectal gland, but not brain, was the increased abundance of several proteins involved in intracellular shuttling of energetic equivalents. The increase in mitochondrial GOT2 after anoxia suggests enhanced unidirectional flux of cytosolic NADH produced in glycolysis to the ETC via the malate aspartate shuttle (15). Such an increase would likely be more important during reoxygenation than anoxia per se, because oxygen limitation would prevent oxidation of NADH and result in an increased mitochondrial NADH:NAD^+ ratio (120). It is also known that GOT2 aids the recovery from ischemia in rat heart (80). Two spots identified as creatine kinase B (CKB) increased after episodic hypoxia, one after H1 and the other after both H1 and H2. Creatine kinase plays a role in the phosphocreatine circuit, which buffers intracellular ATP levels and transfers mitochondrial ATP equivalents throughout the cell (109). Given that this enzyme physically associates with Na^+/K^+-ATPase (28) and plays a role in teleost gill ionoregulation (47), increased CKB following episodic hypoxia may represent increased efficiency of localized ATP buffering to support continued ion pumping function in rectal gland.

Detoxification of Metabolic Byproducts and Amelioration of Oxidative Stress, Particularly in Rectal Gland

Episodic hypoxia induced a number of proteins in the epaulette shark rectal gland for coping with the toxic byproducts of continued metabolic activity during subsequent episodes of oxygen limitation and reoxygenation. These results generally conform with the lack of change in rectal gland Na^+/K^+-ATPase activity following all treatments and the recent "transport at any cost" theory of rectal gland function (110). A variety of proteins involved in the amelioration of oxidative stress increased in rectal gland. Hypoxia elicited more compensatory proteome adjustments in this category than anoxia, consistent with recent evidence for ROS generation [particularly superoxide radical ($O_2^{\cdot}$) and hydrogen peroxide (H_2O_2)] at the electron transport chain during hypoxia (54). The increase in FTH1 after H1 suggests enhanced cellular sequestration of Fe^{2+} ions, most likely to prevent oxygen radical formation via Fenton chemistry (62). The observed increases in COQ5 (↑ H1 and H2) indicate elevated ubiquinone biosynthesis. Ubiquinone has antioxidant properties (55), and it acts as a cofactor for mitochondrial uncoupling proteins that reduce oxygen radical generation at the ETC (20, 34).

Several other rectal gland proteins have more indirect roles in combating oxidative stress. The top-ranking VIP score and most highly upregulated protein for rectal gland, and the only identified protein to change expression in all three treatments in either tissue, was glyoxalase domain containing 5 (GLOD5; ↑ 4.3 × A1, ↑ 3.4 × H1, ↑ 2.9 × H2). Although this particular gene product has not been well characterized, the glyoxalase system detoxifies methylglyoxal, a cytotoxic byproduct of glycolysis (111). Overexpression of glyoxalase I in rat kidneys rescues them from oxidative stress and apoptosis (48). The deubiquitinating enzyme UCHL3 also increased significantly in rectal gland after one episode of hypoxia. This enzyme may function in recycling ubiquitin that was incorrectly bound to GSH or other nucleophiles (68). Finally, although we classified mitochondrial IDH2 (↑ H1) as a TCA cycle enzyme, we propose that it plays more of a role in alleviating mitochondrial oxidative stress than in TCA flux in rectal gland in response to

hypoxia. Recently, IDH2's ability to supply NADPH reducing equivalents (possibly for recycling of GSSG to GSH) was linked to prevention of ROS-mediated apoptosis in response to several stressors (43, 52, 96).

In parallel to the IDH2 hypothesis following hypoxia, expression changes of several rectal gland glycolytic enzymes following anoxia may indicate compensatory adjustments in the oxidative stress response more than changes in energy production. GAPDH abundance increased significantly in rectal gland after anoxia, but glycolytic capacity downstream of GAPDH appears reduced at the same time (TPI1 ↓ after both A1 and H2; PGAM1 ↓ after A1). One possible explanation for this contradictory pattern of expression involves another glycolytic enzyme ALDOB, which tended to increase after both A1 and H1 in the gland (VIP analysis). ALDOB can shuttle glycolytic intermediates into the pentose phosphate pathway, which produces cytosolic reducing equivalents (NADPH) both for biosynthesis and for the GSH ROS-detoxifying system (82). We hypothesize that enhanced retrograde GAPDH activity supplies glyceraldehyde-3-phosphate for conversion by ALDOB into the pentose phosphate shuttle to cope with bursts of ROS production in the gland (54, 56). This mechanism would enhance the oxidative stress response to subsequent episodes of anoxia and reoxygenation.

In the rectal gland, episodic oxygen limitation also induced several proteins with chaperone functions related to oxidative stress. Overexpression of the endoplasmic reticulum (ER) chaperone PPIB (↑ A1 and H1), implicated in adaptation to metabolic and oxidative stress in the kidney (40), inhibits cytosolic Ca^{2+} loading, ROS production, and apoptosis resulting from an excess of unfolded proteins (44). The Parkinson's disease-associated chaperone PARK7 (↑ H1) is induced by oxidative stress and protects rat neurons from such insult (53). Finally, induction by oxidative stress (H_2O_2) of the chaperone DNAJB11/Hsp40 (↑ H1 in rectal gland), a regulator of HSP70 activity, is highly conserved (108). Surprisingly, two members of the HSP70 superfamily were downregulated in rectal gland following anoxia and/or hypoxia (HSPA9 ↓ all treatments; HSPA8 ↓ H1 and H2), suggesting that these chaperones play less of a role in this tissue relative to those that were upregulated.

Proteomic adjustments related to oxidative stress were far less common in cerebellum, including only the highly conserved protein antiquitin (ALDH7A1; ↓ H2) and the inner mitochondrial membrane chaperone PHB (↑ H2) (70). We also observed a decrease in HSPA4L (also known as osmotic stress protein 94) after both H1 and H2 in the cerebellum. In contrast, heat shock proteins are constitutively expressed at high levels in anoxia-tolerant turtle brains and further upregulated to varying degrees during anoxia (83), and they play a role in ischemic preconditioning in mammals (50). Whether ROS production is inherently lower in brain than in rectal gland, antioxidant expression is higher, or tissue-specific changes in substrate utilization lead to varying levels of ROS formation remains to be determined. The total glutathione levels in epaulette shark brain were unexceptional compared with tissues of other fishes (76, 102). In addition, our glutathione data do not indicate dramatic enhancement of the pool of this antioxidant at +24 h, although the consistent changes across control and experimental groups imply that our handling controls worked as designed. Further data, such as activities of glutathione peroxidase and reductase, are needed to determine whether the glutathione system plays a role in the epaulette shark's response to episodic oxygen limitation.

Modulation of Cellular Prosurvival Signaling

It is important to note that transient metabolic depression during episodes of anoxia or hypoxia in epaulette sharks could be mediated by translation-independent mechanisms, particularly posttranslational modifications of existing proteins via signaling cascades, which would not be detected with our experimental design. In our dataset, the abundance of several key signaling proteins changed after episodic hypoxia, but not anoxia, with potential ramifications for metabolic regulation during future periods of oxygen limitation. Adjustments in brain included a transient decrease in the cAMP-dependent protein kinase (PKA) regulatory subunit PRKAR2B after H1, followed by an increase after H2 in another regulatory subunit PRKAR1A. These regulatory subunits bind to the catalytic PKA subunit (PKAc) with different affinities (PRKAR1A binds more tightly, 105) and different sensitivities to cAMP (PRKAR2B more responsive to cAMP, 17). The changing ratio of PRKAR1A to PRKAR2B following episodic hypoxia suggests modulation of PKAc pathways downstream of G protein-coupled receptors (GPCRs), which include glutamate receptors. Furthermore, the GPCR complex member GNAO1, involved in cAMP stimulation of PKA and downstream effects on mitochondrial activity (12), also decreased after H1. PKAc has numerous other downstream targets, including Na^+/K^+-ATPase (3). In contrast, PRKAR1A decreased after H1 in rectal gland, suggesting tissue-specific regulation of the PKA signaling pathway in response to hypoxia. Both tissues also exhibited modulation of several 14-3-3 proteins, which bind phosphorylated signaling proteins and regulate their activity. Both PKA and 14-3-3 signaling cascades represent promising avenues for future research in this species.

An intriguing result in the rectal gland was the upregulation of cystathionase (CTH) after H2. CTH's production of the signaling gas hydrogen sulfide (H_2S) is inversely related to oxygen levels in fish (74), and H_2S formation has very recently been shown to rescue cells from ischemia/reperfusion injury and apoptosis in several tissues (21, 23, 106). The role of CTH and H_2S in hypoxia response in the epaulette shark rectal gland may represent a promising area for further study.

Ultimately, a cell's fate in the face of stressful conditions depends in part on the net balance of pro- and antiapoptotic signaling. In this study, we found no biochemical evidence for increased caspase 3/7-dependent apoptosis in cerebellum or rectal gland at any point following anoxia or hypoxia, nor have previous studies found morphological evidence for apoptosis following repeated hypoxia in the epaulette shark brain (67, 84). We have also found no late apoptotic DNA fragmentation in epaulette shark gill in the same treatments using a TUNEL assay (W. W. Dowd, unpublished observations). These results suggest net prosurvival signaling in epaulette shark tissues during and after periods of oxygen limitation. Accordingly, several proteins potentially involved in antiapoptotic signaling pathways were induced after episodic hypoxia, but not anoxia, in cerebellum. The transcription factor FUBP1 (↑ H2) is required at the promoter of *c-myc*, an oncogene that typically promotes cell cycle progression. We hypothesize that increased

FUBP1 after multiple hypoxic episodes may stimulate a form of *c-myc* "insurance" against programmed cell death (36); *c-myc* may play an analogous role in anoxia-tolerant turtles (26). Two other major players in apoptosis are p53 (generally proapoptotic) and nuclear factor kappa B (NF-κB, generally antiapoptotic). The ubiquitin-conjugating enzyme UBE2D2 (↑ H1 H2) ubiquitinates both p53 and inhibitor of NF-κB (IκB) and targets them for proteasomal degradation, thus releasing antiapoptotic NF-κB for translocation to the nucleus (24). RAN (↑ H1) also plays a role in shuttling of NF-κB to the nucleus (115), and its overexpression protects glioblastoma cells from apoptosis (116). In rectal gland, only the mitochondrial ALDH4A1 increased after H1 here, where it may act as a negative regulator of p53-dependent ROS formation to inhibit apoptosis (119).

Summary

Despite the fact that captive epaulette sharks naïve to oxygen limitation exhibit exceptional intrinsic tolerance at tropical temperatures (13), our data suggest that these sharks enhance a number of compensatory molecular mechanisms in response to episodic hypoxic or anoxic exposure. These tissue and treatment-specific responses should increase the resistance to subsequent episodes of oxygen limitation, and we interpret these compensatory changes as a preconditioned phenotype. In contrast to studies of prolonged hypoxia and anoxia tolerance in other species, episodic oxygen limitation and recovery did not induce sustained metabolic depression in the epaulette shark tissues examined. Rather, these sharks apparently adjust their physiology and proteome to sustain metabolic activity and cope with the consequences, especially following exposure to hypoxia. Because the majority of the observed proteome responses were relatively minor (very few expression ratios >2 or <0.5), the epaulette shark's preconditioning phenotypic response appears quite subtle. We interpret these patterns as fine-tuning of a constitutively expressed suite of compensatory mechanisms that likely evolved under strong selective pressure in the epaulette shark's coral reef habitat.

ACKNOWLEDGMENTS

We are extremely grateful to the staff of Heron Island Research Station, particularly Collette Bagnato and Kate Dunn, for their hospitality and flexibility shortly after much of the Station was lost in a devastating fire. We also thank Adrian Castelli, Dea Olivier, Dion Mulvey, and Selina Ward for assistance with experiments. William Jewell provided extensive support at the UC Davis Campus Mass Spectrometry Facility, and Michelle Dulake assisted with laboratory analyses. The comments of two anonymous reviewers greatly improved the manuscript.

Current address for W. W. Dowd: Hopkins Marine Station of Stanford Univ., 120 Oceanview Blvd., Pacific Grove, CA 93950.

GRANTS

W. W. Dowd was supported by the National Science Foundation (NSF) East Asia and Pacific Summer Institutes Program (OISE-0713887) and the Australian Academy of Science, a Coastal Environmental Quality Initiative Fellowship from the UC Marine Council, an American Elasmobranch Society Student Research Award, a UC Davis Jastro-Shields Research Fellowship, a Society for Integrative and Comparative Biology Grant-in-Aid of Research, and a Marin Rod & Gun Club Scholarship. G. M. C. Renshaw acknowledges support from Sea World Research and Rescue Foundation. The proteomics work was supported by NSF Grant IOS-0542755 and National Institute of Environmental Health Sciences Grant 5 P42 ES-004699 to D. Kültz. Additional support came from UC Agriculture Experiment Station Grant 3455H to J. J. Cech, Jr.

DISCLOSURES

No conflicts of interest, financial or otherwise, are declared by the author(s).

REFERENCES

1. **Arrell DK, Elliott ST, Kane LA, Guo Y, Ko YH, Pedersen PL, Robinson J, Murata M, Murphy AM, Marban E, Van Eyk JE.** Proteomic analysis of pharmacological preconditioning: novel protein targets converge to mitochondrial metabolism pathways. *Circ Res* 99: 706–714, 2006.
2. **Ballantyne JS.** Jaws: the inside story. The metabolism of elasmobranch fishes. *Comp Biochem Physiol* 118B: 703–742, 1997.
3. **Bertorello AM, Aperia A, Walaas SI, Nairn AC, Greengard P.** Phosphorylation of the catalytic subunit of Na^+,K^+-ATPase inhibits the activity of the enzyme. *Proc Natl Acad Sci USA* 88: 11359–11362, 1991.
4. **Bolli R.** The late phase of preconditioning. *Circ Res* 87: 972–983, 2000.
5. **Bosworth CA, Chou CW, Cole RB, Rees BB.** Protein expression patterns in zebrafish skeletal muscle: initial characterization and the effects of hypoxic exposure. *Proteomics* 5: 1362–1371, 2005.
6. **Braithwaite SP, Xia H, Malenka RC.** Differential roles for NSF and GRIP/ABP in AMPA receptor cycling. *Proc Natl Acad Sci USA* 99: 7096–7101, 2002.
7. **Brunner Y, Coute Y, Iezzi M, Foti M, Fukuda M, Hochstrasser DF, Wollheim CB, Sanchez JC.** Proteomics analysis of insulin secretory granules. *Mol Cell Proteomics* 6: 1007–1017, 2007.
8. **Buechler C, Bodzioch M, Bared SM, Sigruener A, Boettcher A, Lapicka-Bodzioch K, Aslanidis C, Duong CQ, Grandl M, Langmann T, Dembinska-Kiec A, Schmitz G.** Expression pattern and raft association of NIPSNAP3 and NIPSNAP4, highly homologous proteins encoded by genes in close proximity to the ATP-binding cassette transporter A1. *Genomics* 83: 1116–1124, 2004.
9. **Calabrese EJ, Bachmann KA, Bailer AJ, Bolger PM, Borak J, Cai L, Cedergreen N, Cherian MG, Chiueh CC, Clarkson TW, Cook RR, Diamond DM, Doolittle DJ, Dorato MA, Duke SO, Feinendegen L, Gardner DE, Hart RW, Hastings KL, Hayes AW, Hoffmann GR, Ives JA, Jaworowski Z, Johnson TE, Jonas WB, Kaminski NE, Keller JG, Klaunig JE, Knudsen TB, Kozumbo WJ, Lettieri T, Liu SZ, Maisseu A, Maynard KI, Masoro EJ, McClellan RO, Mehendale HM, Mothersill C, Newlin DB, Nigg HN, Oehme FW, Phalen RF, Philbert MA, Rattan SIS, Riviere JE, Rodricks J, Sapolsky RM, Scott BR, Seymour C, Sinclair DA, Smith-Sonneborn J, Snow ET, Spear L, Stevenson DE, Thomas Y, Tubiana M, Williams GM, Mattson MP.** Biological stress response terminology: Integrating the concepts of adaptive response and preconditioning stress within a hormetic dose-response framework. *Toxicol Appl Pharmacol* 222: 122–128, 2007.
10. **Calvano S, Xiao W, Richards D, Felciano R, Baker H, Cho R, Chen R, Brownstein B, Cobb J, Tschoeke S, Miller-Graziano C, Moldawer L, Mindrinos M, Davis R, Tompkins R, Lowry S.** Inflamm and Host Response to Injury Large Scale Collab. Res. Program. A network-based analysis of systemic inflammation in humans. *Nature* 437: 1032–1037, 2005.
11. **Canela L, Lujan R, Lluis C, Burgueno J, Mallol J, Canela EI, Franco R, Ciruela F.** The neuronal Ca^{2+}-binding protein 2 (NECAB2) interacts with the adenosine A(2A) receptor and modulates the cell surface expression and function of the receptor. *Mol Cell Neurosci* 36: 1–12, 2007.
12. **Carlucci A, Adornetto A, Scorziello A, Viggiano D, Foca M, Cuomo O, Annunziato L, Gottesman M, Feliciello A.** Proteolysis of AKAP121 regulates mitochondrial activity during cellular hypoxia and brain ischaemia. *EMBO J* 27: 1073–1084, 2008.
13. **Chapman CA, Renshaw GMC.** Hematological responses of the grey carpet shark (*Chiloscyllium punctatum*) and the epaulette shark (*Hemiscyllium ocellatum*) to anoxia and re-oxygenation. *J Exp Zool* 311A: 422–438, 2009.
14. **Da Cruz S, Xenarios I, Langridge J, Vilbois F, Parone PA, Martinou JC.** Proteomic analysis of the mouse liver mitochondrial inner membrane. *J Biol Chem* 278: 41566–41571, 2003.
15. **Dawson AG.** Oxidation of cytosolic NADH formed during aerobic metabolism in mammalian cells. *Trends Biochem Sci* 4: 171–176, 1979.
16. **De Roos R.** Plasma ketone, glucose, lactate, and alanine levels in the vascular supply to and from the brain of the spiny dogfish shark (*Squalus acanthias*). *J Exp Zool* 268: 354–363, 1994.

17. **Diskar M, Zenn HM, Kaupisch A, Prinz A, Herberg FW.** Molecular basis for isoform-specific autoregulation of protein kinase A. *Cell Signal* 19: 2024–2034, 2007.
18. **Dowd WW, Harris BN, Cech JJ Jr, Kültz D.** Proteomic and physiological responses of leopard sharks (*Triakis semifasciata*) to salinity change. *J Exp Biol* 213: 210–224, 2010.
19. **Dowd WW, Wood CM, Kajimura M, Walsh PJ, Kültz D.** Natural feeding influences protein expression in the dogfish shark rectal gland: A proteomic analysis. *Comp Biochem Physiol* 3D: 118–127, 2008.
20. **Echtay KS, Winkler E, Frischmuth K, Klingenberg M.** Uncoupling proteins 2 and 3 are highly active H^+ transporters and highly nucleotide sensitive when activated by coenzyme Q (ubiquinone). *Proc Natl Acad Sci USA* 98: 1416–1421, 2001.
21. **Elrod JW, Calvert JW, Morrison J, Doeller JE, Kraus DW, Tao L, Jiao X, Scalia R, Kiss L, Szabo C, Kimura H, Chow CW, Lefer DJ.** Hydrogen sulfide attenuates myocardial ischemia-reperfusion injury by preservation of mitochondrial function. *Proc Natl Acad Sci USA* 104: 15560–15565, 2007.
22. **Evans DH, Piermarini PM, Choe KP.** Homeostasis: Osmoregulation, pH regulation, and nitrogen excretion. In: *Biology of Sharks and Their Relatives*, edited by Carrier JC, Musick JA, and Heithaus MR. Boca Raton, FL: CRC, 2004, p. 247–268.
23. **Fu Z, Liu X, Geng B, Fang L, Tang C.** Hydrogen sulfide protects rat lung from ischemia-reperfusion injury. *Life Sci* 82: 1196–1202, 2008.
24. **Gonen H, Bercovich B, Orian A, Carrano A, Takizawa C, Yamanaka K, Pagano M, Iwai K, Ciechanover A.** Identification of the ubiquitin carrier proteins, E2s, involved in signal-induced conjugation and subsequent degradation of IκBα. *J Biol Chem* 274: 14823–14830, 1999.
25. **Gray NW, Fourgeaud L, Huang B, Chen J, Cao H, Oswald BJ, Hemar A, McNiven MA.** Dynamin 3 is a component of the postsynapse, where it interacts with mGluR5 and Homer. *Curr Biol* 13: 510–515, 2003.
26. **Greenway SC, Storey KB.** Mitogen-activated protein kinases and anoxia tolerance in turtles. *J Exp Zool* 287: 477–484, 2000.
27. **Grunewald TG, Butt E.** The LIM and SH3 domain protein family: structural proteins or signal transducers or both? *Mol Cancer* 7: 31, 2008.
28. **Guerrero ML, Beron J, Spindler B, Groscurth P, Wallimann T, Verrey F.** Metabolic support of Na+ pump in apically permeabilized A6 kidney cell epithelia: role of creatine kinase. *Am J Physiol Cell Physiol* 272: C697–C706, 1997.
29. **Harris KM, Kater SB.** Dendritic spines: cellular specializations imparting both stability and flexibility to synaptic function. *Annu Rev Neurosci* 17: 341–371, 1994.
30. **Haseloff RF, Krause E, Bigl M, Mikoteit K, Stanimirovic D, Blasig IE.** Differential protein expression in brain capillary endothelial cells induced by hypoxia and posthypoxic reoxygenation. *Proteomics* 6: 1803–1809, 2006.
31. **Hochachka PW, Lutz PL.** Mechanism, origin, and evolution of anoxia tolerance in animals. *Comp Biochem Physiol* 130B: 435–459, 2001.
32. **Hochachka PW, Mommsen TP.** Protons and anaerobiosis. *Science* 219: 1391–1397, 1983.
33. **Hochachka PW, Somero GN.** *Biochemical Adaptation: Mechanism and Process in Physiological Evolution*. New York: Oxford University Press, 2002, p. 466.
34. **Horvath TL, Diano S, Leranth C, Garcia-Segura LM, Cowley MA, Shanabrough M, Elsworth JD, Sotonyi P, Roth RH, Dietrich EH, Matthews RT, Barnstable CJ, Redmond DE Jr.** Coenzyme Q induces nigral mitochondrial uncoupling and prevents dopamine cell loss in a primate model of Parkinson's disease. *Endocrinology* 144: 2757–2760, 2003.
35. **Isono E, Saito N, Kamata N, Saeki Y, Toh EA.** Functional analysis of Rpn6p, a lid component of the 26 S proteasome, using temperature-sensitive rpn6 mutants of the yeast *Saccharomyces cerevisiae*. *J Biol Chem* 280: 6537–6647, 2005.
36. **Jang M, Park BC, Kang S, Chi SW, Cho S, Chung SJ, Lee SC, Bae KH, Park SG.** Far upstream element-binding protein-1, a novel caspase substrate, acts as a cross-talker between apoptosis and the c-myc oncogene. *Oncogene* 28: 1529–1536, 2009.
37. **Johansson D, Nilsson GE, Doving KB.** Anoxic depression of light-evoked potentials in retina and optic tectum of crucian carp. *Neurosci Lett* 237: 73–76, 1997.
38. **John GB, Shang Y, Li L, Renken C, Mannella CA, Selker JM, Rangell L, Bennett MJ, Zha J.** The mitochondrial inner membrane protein mitofilin controls cristae morphology. *Mol Biol Cell* 16: 1543–1554, 2005.
39. **Jorgensen SJ, Klimley AP, Muhlia-Melo AF.** Scalloped hammerhead shark Sphyrna lewini, utilizes deep-water, hypoxic zone in the Gulf of California. *J Fish Biol* 74: 1682–1687, 2009.
40. **Kainer DB, Doris PA.** Cyclophilin B expression in renal proximal tubules of hypertensive rats. *Hypertension* 35: 958–964, 2000.
41. **Kammerer BD, Kültz D.** Prolonged apoptosis in mitochondria-rich cells of tilapia (*Oreochromis mossambicus*) exposed to elevated salinity. *J Comp Physiol* 179B: 535–542, 2009.
42. **Karp NA, Griffin JL, Lilley KS.** Application of partial least squares discriminant analysis to two-dimensional difference gel studies in expression proteomics. *Proteomics* 5: 81–90, 2005.
43. **Kil IS, Kim SY, Lee SJ, Park JW.** Small interfering RNA-mediated silencing of mitochondrial $NADP^+$-dependent isocitrate dehydrogenase enhances the sensitivity of HeLa cells toward tumor necrosis factor-alpha and anticancer drugs. *Free Radic Biol Med* 43: 1197–1207, 2007.
44. **Kim J, Choi TG, Ding Y, Kim Y, Ha KS, Lee KH, Kang I, Ha J, Kaufman RJ, Lee J, Choe W, Kim SS.** Overexpressed cyclophilin B suppresses apoptosis associated with ROS and Ca^{2+} homeostasis after ER stress. *J Cell Sci* 121: 3636–3648, 2008.
45. **Kobayashi S, Millhorn DE.** Hypoxia regulates glutamate metabolism and membrane transport in rat PC12 cells. *J Neurochem* 76: 1935–1948, 2001.
46. **Kültz D.** Molecular and evolutionary basis of the cellular stress response. *Annu Rev Physiol* 67: 225–257, 2005.
47. **Kültz D, Somero GN.** Ion transport in gills of the euryhaline fish *Gillichthys mirabilis* is facilitated by a phosphocreatine circuit. *Am J Physiol Regul Integr Comp Physiol* 268: R1003–R1012, 1995.
48. **Kumagai T, Nangaku M, Kojima I, Nagai R, Ingelfinger JR, Miyata T, Fujita T, Inagi R.** Glyoxalase I overexpression ameliorates renal ischemia-reperfusion injury in rats. *Am J Physiol Renal Physiol* 296: F912–F921, 2009.
49. **Land SC, Hochachka PW.** Protein turnover during metabolic arrest in turtle hepatocytes: role and energy dependence of proteolysis. *Am J Physiol Cell Physiol* 266: C1028–C1036, 1994.
50. **Latchman DS.** Protective effect of heat shock proteins in the nervous system. *Curr Neurovasc Res* 1: 21–27, 2004.
51. **Lee J, Valkova N, White MP, Kültz D.** Proteomic identification of processes and pathways characteristic of osmoregulatory tissues in spiny dogfish shark (*Squalus acanthias*). *Comp Biochem Physiol* 1D: 328–343, 2006.
52. **Lee JH, Kim SY, Kil IS, Park JW.** Regulation of ionizing radiation-induced apoptosis by mitochondrial NADP+-dependent isocitrate dehydrogenase. *J Biol Chem* 282: 13385–13394, 2007.
53. **Lev N, Ickowicz D, Melamed E, Offen D.** Oxidative insults induce DJ-1 upregulation and redistribution: implications for neuroprotection. *Neurotoxicology* 29: 397–405, 2008.
54. **Li C, Jackson RM.** Reactive species mechanisms of cellular hypoxia-reoxygenation injury. *Am J Physiol Cell Physiol* 282: C227–C241, 2002.
55. **Littarru GP, Tiano L.** Bioenergetic and antioxidant properties of coenzyme Q10: recent developments. *Mol Biotechnol* 37: 31–37, 2007.
56. **Lushchak VI, Bagnyukova TV.** Hypoxia induces oxidative stress in tissues of a goby, the rotan *Perccottus glenii*. *Comp Biochem Physiol* 148B: 390–397, 2007.
57. **Lushchak VI, Bagnyukova TV, Lushchak OV, Storey JM, Storey KB.** Hypoxia and recovery perturb free radical processes and antioxidant potential in common carp (*Cyprinus carpio*) tissues. *Int J Biochem Cell Biol* 37: 1319–1330, 2005.
58. **Lutz P, Nilsson GE.** Vertebrate brains at the pilot light. *Respir Physiol Neurobiol* 141: 285–296, 2004.
59. **Lutz PA, Nilsson GE, Prentice HM.** *The Brain Without Oxygen: Causes of Failure - Physiological and Molecular Mechanisms for Survival*. Dordrecht, The Netherlands: Kluwer Academic, 2003.
60. **Ma B, Zhang K, Hendrie C, Liang C, Li M, Doherty-Kirby A, Lajoie G.** PEAKS: Powerful software for peptide *de novo* sequencing by tandem mass spectrometry. *Rapid Commun Mass Spectrom* 17: 2337–2342, 2003.
61. **MacDonald JA, Storey KB.** Regulation of ground squirrel Na^+K^+-ATPase activity by reversible phosphorylation during hibernation. *Biochem Biophys Res Commun* 254: 424–429, 1999.
62. **MacKenzie EL, Iwasaki K, Tsuji Y.** Intracellular iron transport and storage: from molecular mechanisms to health implications. *Antioxid Redox Signal* 10: 997–1030, 2008.

63. **Matey V, Wood CM, Dowd WW, Kültz D, Walsh PJ.** Morphology of the rectal gland of the spiny dogfish (*Squalus acanthias*) shark in response to feeding. *Can J Zool* 87: 440–452, 2009.
64. **McCormick SD.** Methods for nonlethal gill biopsy and measurement of Na+, K+-ATPase activity. *Can J Fish Aquat Sci* 50: 656–658, 1993.
65. **Meller R, Thompson SJ, Lusardi TA, Ordonez AN, Ashley MD, Jessick V, Wang W, Torrey DJ, Henshall DC, Gafken PR, Saugstad JA, Xiong ZG, Simon RP.** Ubiquitin proteasome-mediated synaptic reorganization: a novel mechanism underlying rapid ischemic tolerance. *J Neurosci* 28: 50–59, 2008.
66. **Milton SL, Prentice HM.** Beyond anoxia: The physiology of metabolic downregulation and recovery in the anoxia-tolerant turtle. *Comp Biochem Physiol* 147A: 277–290, 2007.
67. **Mulvey JM, Renshaw GMC.** GABA is not elevated during neuroprotective neuronal depression in the hypoxic epaulette shark (*Hemiscyllium ocellatum*). *Comp Biochem Physiol* 152A: 273–277, 2009.
68. **Mulvey JM, Renshaw GMC.** Neuronal oxidative hypometabolism in the brainstem of the epaulette shark (*Hemiscyllium ocellatum*) in response to hypoxic pre-conditioning. *Neurosci Lett* 290: 1–4, 2000.
69. **Nägerl UV, Eberhorn N, Cambridge SB, Bonhoeffer T.** Bidirectional activity-dependent morphological plasticity in hippocampal neurons. *Neuron* 44: 759–767, 2004.
70. **Nijtmans LGJ, de Jong L, Artal Sanz M, Coates PJ, Berden JA, Back JW, Muijsers AO, van der Spek H, Grivell LA.** Prohibitins act as a membrane-bound chaperone for the stabilization of mitochondrial proteins. *EMBO J* 19: 2444–2451, 2000.
71. **Nilsson GE, Renshaw GMC.** Hypoxic survival strategies in two fishes: extreme anoxia tolerance in the North European crucian carp and natural hypoxic reconditioning in a coral-reef shark. *J Exp Biol* 207: 3131–3139, 2004.
72. **Okamoto H, Nagai T, Miyawaki A, Hayashi Y.** Rapid and persistent modulation of actin dynamics regulates postsynaptic reorganization underlying bidirectional plasticity. *Nat Neurosci* 10: 1104–1112, 2004.
73. **Okamoto K, Bosch M, Hayashi Y.** The roles of CaMKII and F-Actin in the structural plasticity of dendritic spines: a potential molecular identity of a synaptic tag? *Physiology* 24: 357–366, 2009.
74. **Olson KR, Healy MJ, Qin Z, Skovgaard N, Vulesevic B, Duff DW, Whitfield NL, Yang G, Wang R, Perry SF.** Hydrogen sulfide as an oxygen sensor in trout gill chemoreceptors. *Am J Physiol Regul Integr Comp Physiol* 295: R669–R680, 2008.
75. **Palermo G, Piraino P, Zucht HD.** Performance of PLS regression coefficients in selecting variables for each response of a multivariate PLS for omics-type data. *Adv Appl Bioinform Chem* 2: 57–70, 2009.
76. **Pandey S, Parvez S, Sayeed I, Haque R, Bin-Hafeez B, Raisuddin S.** Biomarkers of oxidative stress: a comparative study of river Yamuna fish *Wallago attu* (Bl. & Schn). *Sci Total Environ* 309: 105–115, 2003.
77. **Parnas I, Rashkovan G, O'Connor V, El-Far O, Betz H, Parnas H.** Role of NSF in neurotransmitter release: a peptide microinjection study at the crayfish neuromuscular junction. *J Neurophysiol* 96: 1053–1060, 2006.
78. **Pérez-Enciso M, Tenenhaus M.** Prediction of clinical outcome with microarray data: a partial least squares discriminant analysis (PLS-DA) approach. *Hum Genet* 112: 581–592, 2003.
79. **Perkins DN, Pappin DJC, Creasy DM, Cottrell JS.** Probability-based protein identification by searching sequence databases using mass spectrometry data. *Electrophoresis* 20: 3551–3567, 1999.
79a. **Piermarini PM, Evans DH.** Effects of environmental salinity on Na^+/K^+-ATPase in the gills and rectal gland of a euryhaline elasmobranch (Dasyatis sabina). *J Exp Biol* 203: 2957–2966, 2000.
80. **Pisarenko OI, Studneva IM, Shulzhenko VS, Korchazhkina OV, Kapelko VI.** Substrate accessibility to cytosolic aspartate aminotransferase improves posthypoxic recovery of isolated rat heart. *Biochem Mol Med* 55: 138–148, 1995.
81. **Podrabsky JE, Lopez JP, Fan TWM, Higashi R, Somero GN.** Extreme anoxia tolerance in embryos of the annual killifish Austrofundulus limnaeus: insights from a metabolomics analysis. *J Exp Biol* 210: 2253–2266, 2007.
82. **Prendes MG, Gonzalez MS, Torresin ME, Hermann R, Pascale NG, Del Mar Jaitovich M, Savino EA, Varela A.** Involvement of mitochondrial permeability transition, glutathione status, pentose phosphate pathway, and oxidative damage in the protective effect of fasting on the ischaemic-reperfused rat heart. *Clin Exp Pharmacol Physiol* 28: 637–642, 2008.
83. **Prentice HM, Milton SL, Scheurle D, Lutz PL.** The upregulation of cognate and inducible heat shock proteins in the anoxic turtle brain. *J Cereb Blood Flow Metab* 24: 826–828, 2004.
84. **Renshaw GMC, Dyson SE.** Increased nitric oxide synthase in the vasculature of the epaulette shark brain following hypoxia. *Neuroreport* 10: 1707–1712, 1999.
85. **Renshaw GMC, Kerrisk CB, Nilsson GE.** The role of adenosine in the anoxic survival of the epaulette shark, *Hemiscyllium ocellatum*. *Comp Biochem Physiol* 131B: 133–141, 2002.
86. **Ringstad N, Nemoto Y, De Camilli P.** The SH3p4/Sh3p8/SH3p13 protein family: binding partners for synaptojanin and dynamin via a Grb2-like Src homology 3 domain. *Proc Natl Acad Sci USA* 94: 8569–8574, 1997.
87. **Rizvi A, Tang XL, Qiu Y, Xuan YT, Takano H, Jadoon AK, Bolli R.** Increased protein synthesis is necessary for the development of late preconditioning against myocardial stunning. *Am J Physiol Heart Circ Physiol* 277: H874–H884, 1999.
88. **Rolfe DF, Brown GC.** Cellular energy utilization and molecular origin of standard metabolic rate in mammals. *Physiol Rev* 77: 731–758, 1997.
89. **Routley MH, Nilsson GE, Renshaw GMC.** Exposure to hypoxia primes the respiratory and metabolic responses of the epaulette shark to progressive hypoxia. *Comp Biochem Physiol* 131A: 313–321, 2002.
90. **Saba H, Batinic-Haberle I, Munusamy S, Mitchell T, Lichti C, Megyesi J, MacMillan-Crow LA.** Manganese porphyrin reduces renal injury and mitochondrial damage during ischemia/reperfusion. *Free Radic Biol Med* 42: 1571–1578, 2007.
91. **Said HM, Hagemann C, Stojic J, Schoemig B, Vince GH, Flentje M, Roosen K, Vordermark D.** GAPDH is not regulated in human glioblastoma under hypoxic conditions. *BMC Mol Biol* 8: 55, 2007.
92. **Santamaria PG, Finley D, Ballesta JP, Remacha M.** Rpn6p, a proteasome subunit from *Saccharomyces cerevisiae*, is essential for the assembly and activity of the 26 S proteasome. *J Biol Chem* 278: 6687–6695, 2003.
93. **Sarabi AS, Shen H, Wang Y, Hoffer BJ, Bäckman CM.** Gene expression patterns in mouse cortical penumbra after focal ischemic brain injury and reperfusion. *J Neurosci Res* 86: 2912–2924, 2008.
94. **Schmidt U, Im KB, Benzing C, Janjetovic S, Rippe K, Lichter P, Wachsmuth M.** Assembly and mobility of exon-exon junction complexes in living cells. *RNA* 15: 862–876, 2009.
95. **Seta K, Kim HW, Ferguson T, Kim R, Pathrose P, Yuan Y, Lu G, Spicer Z, Millhorn DE.** Genomic and physiological analysis of oxygen sensitivity and hypoxia tolerance in PC12 cells. *Ann NY Acad Sci* 971: 379–388, 2002.
96. **Shin SW, Kil IS, Park JW.** Silencing of mitochondrial $NADP^+$-dependent isocitrate dehydrogenase by small interfering RNA enhances heat shock-induced apoptosis. *Biochem Biophys Res Commun* 366: 1012–1018, 2008.
97. **Sick TJ, Perez-Pinon M, Lutz PL, Rosenthal M.** Maintaining coupled metabolism and membrane function in anoxic brain: a comparison between the turtle and rat. In: *Surviving Hypoxia*, edited by Hochachka PW, Lutz PL, Sick T, Rosenthal M, van den Thillart G. Boca Raton, FL: CRC, 1993, p. 351–363.
98. **Staples JF, Buck LT.** Matching cellular metabolic supply and demand in energy-stressed animals. *Comp Biochem Physiol* 153A: 95–105, 2009.
99. **Stein AB, Tang XL, Guo Y, Xuan YT, Dawn B, Bolli R.** Delayed adaptation of the heart to stress: late preconditioning. *Stroke* 35: 2676–2679, 2006.
100. **Stenbeck G.** Soluble NSF-attachment proteins. *Int J Biochem Cell Biol* 30: 573–577, 1998.
101. **Stensløkken KO, Milton SL, Lutz PL, Sundin L, Renshaw GMC, Stecyk JAW, Nilsson GE.** Effect of anoxia on the electroretinogram of three anoxia-tolerant vertebrates. *Comp Biochem Physiol* 150A: 395–403, 2008.
102. **Stephensen E, Sturve J, Förlin L.** Effects of redox cycling compounds on glutathione content and activity of glutathione-related enzymes in rainbow trout liver. *Comp Biochem Physiol* 133A: 435–442, 2002.
103. **Suzue T, Wu GB, Furukawa T.** High susceptibility to hypoxia of afferent synaptic transmission in the goldfish sacculus. *J Neurophysiol* 58: 1066–1079, 1987.
104. **Tauskela JS, Brunette E, Monette R, Comas T, Morley P.** Preconditioning of cortical neurons by oxygen-glucose deprivation: tolerance induction through abbreviated neurotoxic signaling. *Am J Physiol Cell Physiol* 285: C899–C911, 2003.

105. **Taylor SS, Kim C, Vigil D, Haste NM, Yang J, Wu J, Anand GS.** Dynamics of signaling by PKA. *Biochim Biophys Acta* 1754: 25–37, 2005.
106. **Tripatara P, Patel NS, Brancaleone V, Renshaw D, Rocha J, Sepodes B, Mota-Filipe H, Perretti M, Thiemermann C.** Characterisation of cystathionine gamma-lyase/hydrogen sulphide pathway in ischaemia/reperfusion injury of the mouse kidney: an in vivo study. *Eur J Pharmacol* 606: 205–209, 2009.
107. **Valkova N, Yunis R, Mak S, Kang K, Kültz D.** Nek8 mutation causes overexpression of galectin-1, sorcin, and vimentin and accumulation of the major urinary protein in renal cysts of jck mice. *Mol Cell Proteomics* 4: 1009–1018, 2005.
108. **Vandenbroucke K, Robbens S, Vandepoele K, Inze D, Van de Peer Y, Van Breusegem F.** Hydrogen peroxide-induced gene expression across kingdoms: a comparative analysis. *Mol Biol Evol* 25: 507–516, 2008.
109. **Wallimann T, Wyss M, Brdiczka D, Nicolay K, Eppenberger HM.** Intracellular compartmentation, structure and function of creatine kinase isoenzymes in tissues with high and fluctuating energy demands: the 'phosphocreatine circuit' for cellular energy homeostasis. *Biochem J* 281 21–40, 1992.
110. **Walsh PJ, Kajimura M, Mommsen TP, Wood CM.** Metabolic organization and effects of feeding on enzyme activities of the dogfish shark (*Squalus acanthias*) rectal gland. *J Exp Biol* 209: 2929–2938, 2006.
111. **Wang H, Liu J, Wu L.** Methylglyoxal-induced mitochondrial dysfunction in vascular smooth muscle cells. *Biochem Pharmacol* 77: 1709–1716, 2009.
112. **Wieser W, Krumschnabel G.** Hierarchies of ATP-consuming processes: direct compared with indirect measurements, and comparative aspects. *Biochem J* 355: 389–395, 2001.
113. **Wise G, Mulvey JM, Renshaw GMC.** Hypoxia tolerance in the epaulette shark (*Hemiscyllium ocellatum*). *J Exp Zool* 281: 1–5, 1998.
114. **Wold S, Sjöström M, Eriksson L.** PLS-regression: a basic tool of chemometrics. *Chemometr Intell Lab Syst* 58: 109–130, 2001.
115. **Wong CH, Chan H, Ho CY, Lai SK, Chan KS, Koh CG, Li HY.** Apoptotic histone modification inhibits nuclear transport by regulating RCC1. *Nat Cell Biol* 11: 36–45, 2009.
116. **Woo IS, Jang HS, Eun SY, Kim HJ, Ham SA, Kim HJ, Lee JH, Chang KC, Kim JH, Han CW, Seo HG.** Ran suppresses paclitaxel-induced apoptosis in human glioblastoma cells. *Apoptosis* 13: 1223–1231, 2008.
117. **Wulff T, Hoffmann EK, Roepstorff P, Jessen F.** Comparison of two anoxia models in rainbow trout cells by a 2-DE and MS/MS-based proteome approach. *Proteomics* 8: 2035–2044, 2008.
118. **Xu C, Zhang X, Yu C, Lu G, Chen S, Xu L, Ding W, Shi Q, Li Y.** Proteomic analysis of hepatic ischemia/reperfusion injury and ischemic preconditioning in mice revealed the protective role of ATP5beta. *Proteomics* 9: 409–419, 2009.
119. **Yoon KA, Nakamura Y, Arakawa H.** Identification of ALDH4 as a p53-inducible gene and its protective role in cellular stresses. *J Hum Genet* 49: 134–140, 2004.
120. **Zhou L, Stanley WC, Saidel GM, Yu X, Cabrera ME.** Regulation of lactate production at the onset of ischaemia is independent of mitochondrial NADH/NAD^+: insights from in silico studies. *J Physiol* 569: 925–937, 2005.
121. **Zick M, Rabl R, Reichert AS.** Cristae formation-linking ultrastructure and function of mitochondria. *Biochim Biophys Acta* 1793: 5–19, 2009.